In Situ measurements of environmental gamma radiation using a mobile Ge(Li) spectrometer system

Nielsen, Sven Poul

Publication date:
1977

Document Version
Publisher's PDF, also known as Version of record

Risø Report No. 367

Risø Report No. 367

Risø National Laboratory

In Situ Measurements of Environmental Gamma Radiation Using a Mobile Ge(Li) Spectrometer System

by S. P. Nielsen

November 1977

Sales distributors: Jul. Gjellerup, Sølvgade 87, DK-1307 Copenhagen K, Denmark

Available on exchange from: Risø Library, Risø National Laboratory, P.O. Box 49, DK-4000 Roskilde, Denmark

INIS Descriptors

BACKGROUND RADIATION
CALIBRATION
CESIUM 137
COMPUTER CALCULATIONS
COSMIC RADIATION
DENMARK
DOSE RATES
ENVIRONMENT
GAMMA RADIATION
GAMMA DETECTION
GAMMA SPECTROSCOPY
GLOBAL FALLOUT
IONIZATION CHAMBERS
LI-DRIFTED GE DETECTORS
POTASSIUM 40
RADIOACTIVITY
RADIUM 226
RADON 222
SODIUM IODIDES
SOILS
THALLIUM
THORIUM 232
URANIUM 238

UDC 614.73 : 539.122.164

November 1977 Risø Report No. 367

In Situ Measurements of Environmental Gamma Radiation Using a Mobile Ge(Li) Spectrometer System

by

S.P. Nielsen

Risø National Laboratory
Health Physics Department

Abstract

A description is given of the setting up of a mobile Ge(Li) spectrometer system for field measurements of environmental gamma radiation. A computer program was worked out for the processing of the recorded Ge(Li) spectra and the program performance evaluated from analyses of test spectra provided by the International Atomic Energy Agency. The validity of the results from the spectrometer system was assessed from a series of measurements at a single locality and from a series of country-wide measurements. The results from the field measurements of the radionuclide concentrations in the soil were compared to the results of laboratory measurements of collected soil samples. The estimates of the exposure rates from the individual radionuclides were compared to the results of measurements of the total exposure rate.

This report is submitted to the Technical University of Denmark in partial fulfilment of the requirements for obtaining the lic.tech. (Ph.D.) degree.

ISBN 87-550-0501-2

ISSN 0418-6443

CONTENTS

ABBREVIATIONS AND UNITS

keV	10^3 electron volts
MeV	10^6 electron volts
pCi	picocurie, 10^{-12} Ci
mCi	millicurie, 10^{-3} Ci
μR	micro-roentgen, 10^{-6} R
cps	counts per second
ϕ	uncollided gamma flux, photons/cm^2/s
$\dot{X}$	exposure rate, μR/h
μ	linear attenuation coefficient, cm^2/g
ρ	density, g/cm^3
f	gamma yield, photons/disintegration
α	reciprocal relaxation length for exponential distribution, cm^{-1}
σ	standard deviation
S.D.	standard deviation, $\sqrt{\frac{(\bar{x}-x_i)^2}{n-1}}$
S.E.	standard error, $\sqrt{\frac{(\bar{x}-x_i)^2}{n(n-1)}}$

1. INTRODUCTION

Environmental gamma radiation originates partly from naturally occurring radionuclides and partly from man-made radionuclides in the form of fallout from atmospheric nuclear weapons tests. Field measurements of environmental gamma radiation with Ge(Li) spectrometer systems yield detailed information on the presence of gamma-emitting radionuclides in the soil and permit assessments of radionuclide concentrations and exposure rates. With such mobile systems it is possible to detect even the presence of trace amounts of man-made radionuclides in the environment, and several countries now employ similar equipment in the control of environmental pollution from nuclear power stations.

Concerning the determination of radionuclide concentrations in the soil, field measurements have a considerable advantage compared to laboratory measurements of collected soil samples, because the detector in a field measurement registers the radiation from several tons of soil, while the amount of soil in a sample is for practical reasons restricted to a few kilograms in weight. The results from a field measurement are therefore more representative of the site being measured than the results of laboratory measurements. In addition the counting time of a field measurement needs only to be about one tenth of that of a laboratory measurement to obtain the same statistical precision.

Quantitative measurements of penetrating environmental radiation from terrestrial sources and from secondary cosmic radiation were first made with portable ionization chambers[1,2]. Later, field gamma spectroscopy using NaI(Tl) detectors made it possible to qualitatively and quantitatively determine the major contributors to environmental gamma radiation and to relate individual exposure rates to radionuclide concentrations[3-6]. This technique was highly improved by the advent of portable large Ge(Li) detectors, whose superior resolution of gamma-ray energies more than adequately compensated for the lower detection efficiency compared to NaI(Tl) detectors[7-11].

The present report describes the setting up of a mobile Ge(Li) spectrometer system. The results of the calibration of the detector system are presented and a description is given of a computer program prepared for the processing of the recorded

gamma-ray spectra. Finally, the results of measurements made throughout the country are given, and the validity of the results is investigated by comparing with the results from laboratory measurements of collected soil samples and with the results from measurements of the total exposure rates in air.

2. EQUIPMENT

2.1. Installations in Motor Vehicle

The van-type motor vehicle is especially equipped for transport of the spectrometer system and to provide electrical power for the instruments. The installations are shown schematically in fig. 2.1.1.

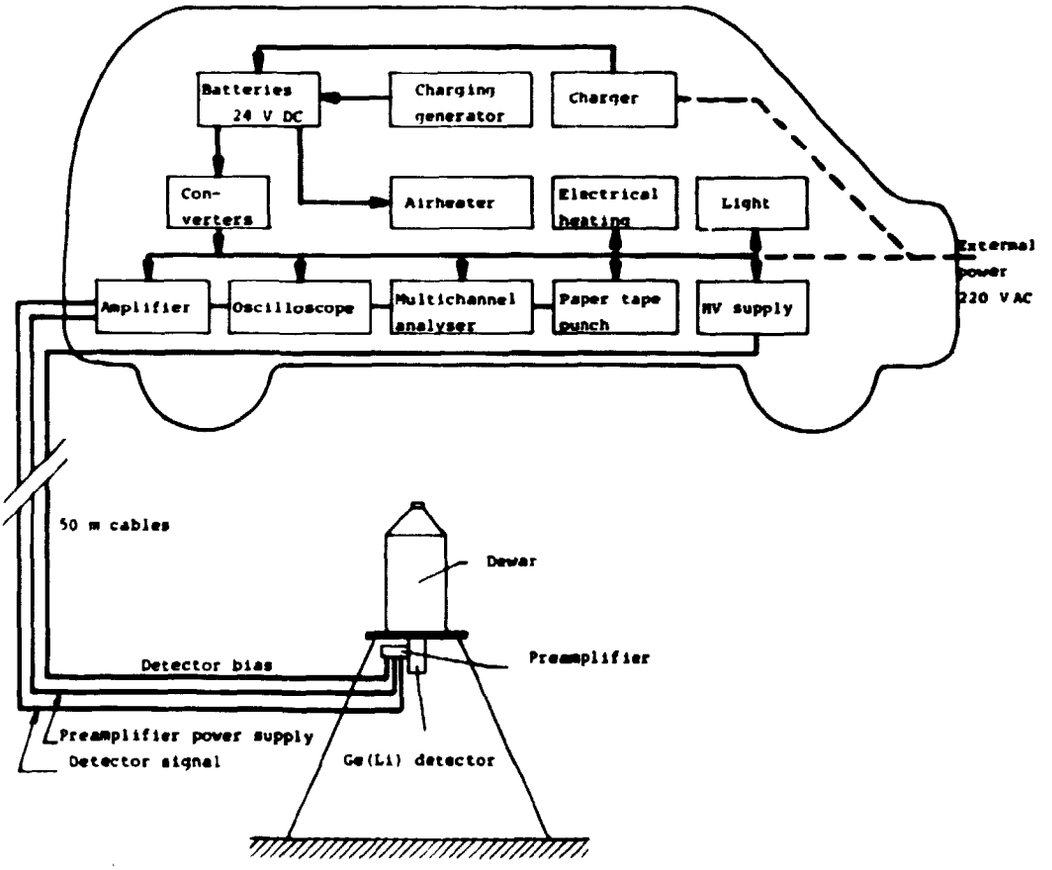

Fig. 2.1.1. Schematic diagram of equipment.

The source of power is two 12-volt batteries of 208 ampere-hours connected in series. The DC voltage is converted to 220 V AC. Two independant converters are installed, each with a power of 500 watts, and this is sufficient to supply the electronics during measurements. The batteries are charged either from an automatic charging unit using external power, which can also supply the instruments directly, or from a special charging generator coupled to the vehicle engine. With fully-charged batteries the DC-AC converter system provides a maximum of 6 hours operation without simultaneous charging.

The vehicle is heated by means of a thermostat-controlled airheater, consuming diesel oil, or by an electrical heating element used when external power is available.

The dimensioning of the electrical power system allows for the operation of other and more power-consuming systems than the spectrometer system, which thereby increases the applicability of the motor vehicle.

2.2. Electronic Instruments for the Spectrometer System

As shown in fig. 2.1.1, the detector system is connected to the electronics through 50 m long cables which permit the detector set-up to be placed sufficiently far away from the vehicle to avoid unwanted shielding effects. The cables supply the detector with high voltage, the preamplifier with power and return the detector signal to the main amplifier. Here the pulses are shaped for subsequent analysis in the multichannel analyser, which has a 4k memory. Limited analysis can be performed in the field of the accumulated spectra using the inherent integrating capabilities of the analyser, but as the detailed analysis is made by computer, the spectra are punched on paper tape and transferred to the B6700 computer at Risø.

The instruments are mounted in wooden boxes secured to a table in the vehicle and are thus easily transportable for use in the laboratory.

2.3. Ge(Li) Detector System

The Ge(Li) detector is mounted vertically in a cryostat of common vacuum type underneath the liquid nitrogen dewar flask, fig. 2.1.1. The detector is of the closed-end, coaxially-drifted type; it has a resolution of 2.0 keV fwhm (full width

at half maximum) at 1.33 MeV, and a full energy peak efficiency of 17% relative to a 7.5 x 7.5 cm NaI(Tl) detector. The pre-amplifier, which has an uncooled field effect transistor, is permanently mounted on the side of the cryostat.

When measuring in the field, the detector system is placed on a tripod with the center of the detector 1 m above ground. Field spectra are accumulated with a gain of 0.7 keV/channel making full use of the 4k memory of the analyser for energies below 2.8 MeV.

The dewar flask has a volume of 15 l and requires refilling less than once a week. With an extra 50 l dewar flask carried in the vehicle, operations can be maintained for three weeks before new supplies of liquid nitrogen are needed. During transportation in the vehicle the detector system is placed on shock absorbers in order to minimize mechanical stresses.

2.4. NaI(Tl) Detector

A 7.5 x 7.5 cm NaI(Tl) scintaillation detector is used to provide independent measurements for comparison with the Ge(Li) detector measurements.

The detector is placed in a tin canister lined with 5 cm expanded polystyrene to reduce the influence of temperature variations on the photomultiplier tube. During measurements the detector is placed on a tripod 1 m above ground and connected to the vehicle instrumentation through the 50 m cables. The resolution of the detector measured at 1.33 MeV is 8.0% fwhm and the spectra are therefore satisfactorily accumulated with a gain of 25 keV/channel, permitting each spectrum to be recorded in 125 channels.

2.5. High Pressure Ionization Chamber

An argon-filled high pressure ionization chamber system recording exposure rates is used to supplement the spectrometric measurements. The ionization chamber system was purchased from Reuter Stokes, USA, and was developed at the Health and Safety Laboratory[12]. Minor changes have been made to the system in order to facilitate the transfer of data from the magnetic tape recording system to the B6700 computer.

3. BASIS OF SPECTRUM EVALUATION

The gamma radiation field at ground level consists mainly of scattered gamma rays originating from decaying radionuclides in the soil. In a field measurement, the instrumentation produces a gamma spectrum, which is a projection of the gamma-ray energy distribution at the detector. The scattered gamma rays, which are detected, have lost part of their initial energy because of the attenuating properties of the soil, of the air and of the detector, and these gamma rays yield the background that slowly varies with energy in the spectrum. A minor fraction of the total number of detected gamma rays travels directly from the decaying nuclei in the soil to the detector and deposits all the initial energy, thereby producing the peaks in the spectrum. The positions and intensities of these peaks (full energy peaks) give information on the identities and quantities of the gamma-emitting radionuclides in the soil. Examples of field spectra are shown in fig. 3.1.

3.1. Ge(Li) Spectrum Evaluation

The Ge(Li) spectrum evaluation is based on a technique developed by Beck[7]. The basic principle involved is the fact that the count rates of the full energy peaks in the spectrum are proportional to the concentrations of and the exposure rates from the corresponding gamma emitters in the soil.

According to this principle, simple conversion factors are calculated for each peak in the spectrum, and these energy-dependant factors take account of the angular distribution of the uncollided gamma rays, of the detector efficiency, and of the uncollided gamma flux from the sources in the soil. This is expressed in the equation:

$$\frac{N_f}{S} = \frac{N_f}{N_o} \cdot \frac{N_o}{\phi} \cdot \frac{\phi}{S} , \qquad (3.1.1)$$

where N_f is the count rate (cps) for the full energy peaks, S the radionuclide concentration in the soil (pCi/g or mCi/km^2), N_o the count rate (cps) of the full energy peaks from gamma rays emitted directly underneath the detector, and ϕ the uncollided gamma flux (photons/cm^2/s) 1 m above ground.

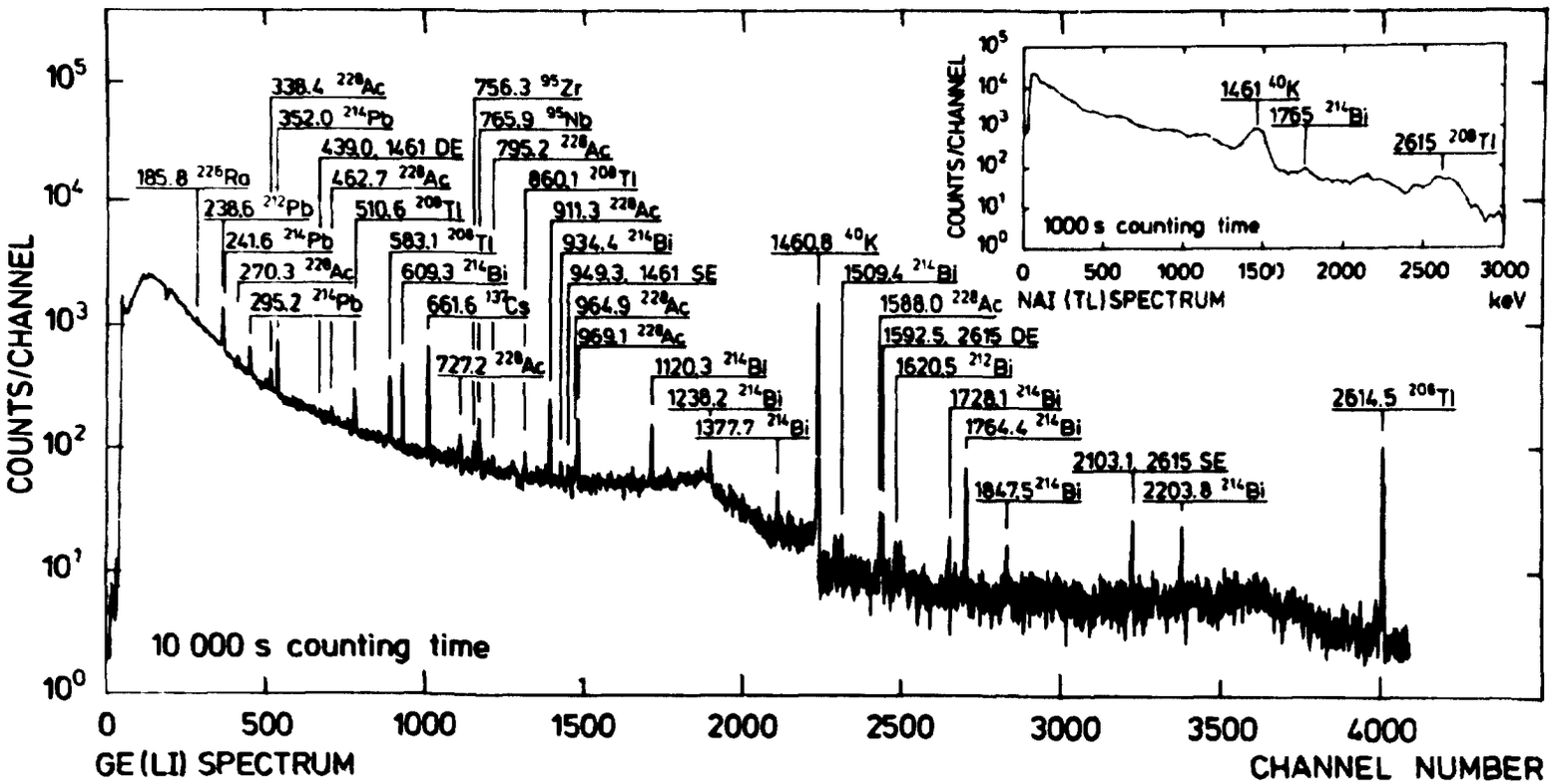

Fig. 3.1. Examples of field spectra (Tystofte, uncultivated soil).

The ratio of the full energy peak count rate to the exposure rate $N_f/\dot{X}$ is obtained by replacing S by $\dot{X}$ (μR/h) in equation (3.1.1).

The naturally occurring radionuclides, table 3.1.1, are assumed to be homogeneously distributed in the soil. Fresh fallout is assumed to represent a plane source evenly deposited on the surface of the soil, while the concentration of aged fallout in the soil is assumed to decrease exponentially with depth[14].

Table 3.1.1

Some important characteristics of ^{40}K and of the ^{238}U and ^{232}Th decay chains

Nuclide	Radiation	Half-life	Nuclide	Radiation	Half-life
^{238}U (UI)	α	$4.5 \cdot 10^9$y	^{232}Th	α	$1.40 \cdot 10^{10}$y
^{234}Th (UX_1)	β^-	24.1d	^{228}Ra ($MsTh_1$)	β^-	5.75y
^{234m}Pa (UX_2)	β^-	1.18m	^{228}Ac ($MsTh_2$)	β^-	6.13h
^{234}U (UII)	α	$2.5 \cdot 10^5$y	^{228}Th (RdTh)	α	1.91y
^{230}Th (J_o)	α	$8 \cdot 10^4$y	^{224}Ra (ThX)	α	3.64d
^{226}Ra	α	1600y	^{220}Rn (thoron)	α	55.3s
^{222}Rn (radon)	α	3.82d	^{216}Po (ThA)	α	0.15s
^{218}Po (RaA)	α	3.05m	^{212}Pb (ThB)	β^-	10.64h
^{214}Pb (RaB)	β^-	26.8m	^{212}Bi (ThC)	α (36%) β^- (64%)	60.6m
^{214}Bi (RaC)	β^-	19.8m			
^{214}Po (RaC')	α	$1.6 \cdot 10^{-4}$s	^{212}Po (ThC') 36%	α	$3 \cdot 10^{-7}$s
^{210}Tl (RaC")	β^-	1.5m	^{208}Tl (ThC") 64%	β^-	3.1m
^{210}Pb (RaD)	β^-	21.3y	^{208}Pb		-
^{210}Bi (RaE)	β^-	5.01d			
^{210}Po (RaF)	α	138.4d	^{40}K	β^-, EC	$1.28 \cdot 10^9$y
^{206}Pb	stable	-			

3.1.1. Correction Factor for Angular Dependence, N_f/N_o

N_f/N_o is the full energy peak count rate from a distributed source in a field measurement relative to that if the source were directly underneath the detector. Assuming a cylinder-symmetric detector response, N_f/N_o is calculated according to:

$$\frac{N_f}{N_o} = \frac{\int_0^{\pi/2} R(\theta) \frac{d\phi}{d\theta} d\theta}{\int_0^{\pi/2} \frac{d\phi}{d\theta} d\theta} \qquad (3.1.1.1)$$

where $R(\theta)$ is the angular response of the detector determined with point sources and $\frac{d\phi}{d\theta}$ is the differential uncollided gamma flux 1 m above ground.

3.1.2. Full Energy Peak Efficiency, N_o/ϕ

The full energy peak efficiency of the detector, N_o/ϕ, is calculated from measurements performed by placing absolutely calibrated point sources directly underneath the detector, thus providing a parallel beam of gamma rays incident on the detector.

3.1.3. Uncollided Gamma Flux per Unit Concentration of Source, ϕ/S

The uncollided gamma flux 1 m above ground per unit concentration of source, ϕ/S, is calculated from the schematic model shown in fig. 3.1.3.1.

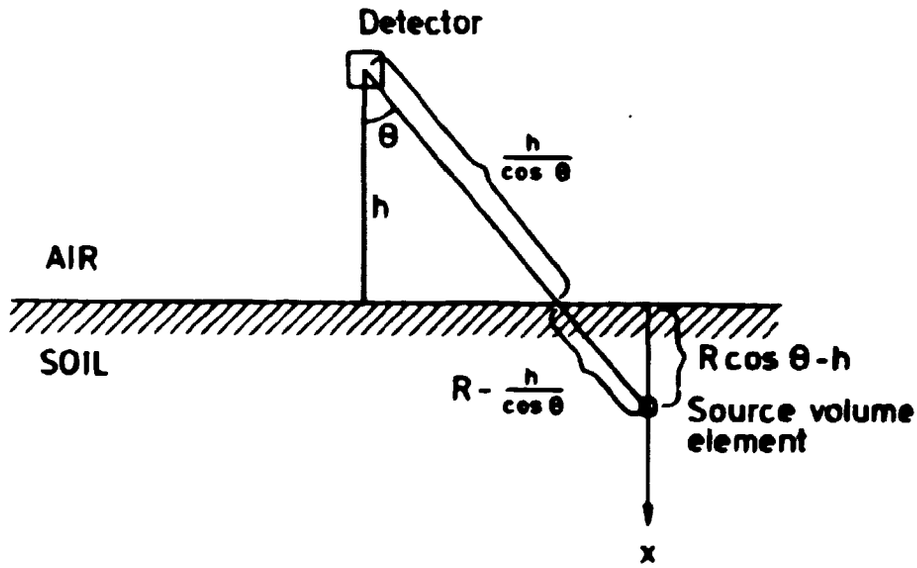

Fig. 3.1.3.1. Schematic model for the calculation of ϕ/S.

The detector is situated a distance h above the infinite plane interface between the two media that have the linear attenuation coefficients μ_a and μ_s and the densities ρ_a and ρ_s, where the indices a and s refer to air and soil, respectively. The source concentrations are assumed to decrease exponentially with depth:

$$S(x) = S_o \exp[-(\alpha/\rho_s) x \rho_s], \qquad (3.1.3.1)$$

where S(x) is the radionuclide activity per unit volume at depth x in the soil, S_o the corresponding surface concentration and α the reciprocal of the relaxation length. The distribution is conveniently characterized by the depth distribution parameter α/ρ_s. The total source concentration per unit area, S_A, is obtained:

$$S_A = \int_o^\infty S(x)\, dx = S_o/\alpha. \qquad (3.1.3.2)$$

The total uncollided flux ϕ from a monoenergetic gamma emitter is given by:

$$\phi = \int_o^{\pi/2} \int_{\frac{h}{\cos\theta}}^{\infty} S_o(4\pi R^2)^{-1} \exp[-(\alpha/\rho_s)(R\cos\theta - h)\rho_s] \cdot$$

$$\exp[-(\mu_a/\rho_a)h\rho_a/\cos\theta - (\mu_s/\rho_s)(R - h/\cos\theta)\rho_s]\, 2\pi R^2 \sin\theta\, dR\, d\theta, \qquad (3.1.3.3)$$

where R is the distance from the detector to the infinitesimal volume element and θ the angle between the R-vector and vertical.

The integration of this equation is described in detail in the appendix and only the results are given here.

The R-integration yields:

$$\frac{d\phi}{d\theta} = \frac{S_o \sin\theta \exp[-(\mu_a/\rho_a)h\rho_a/\cos\theta]}{2[(\alpha/\rho_s)\cos\theta + (\mu_s/\rho_s)]\rho_s}, \qquad (3.1.3.4)$$

and the θ-integration:

$$\phi = (S_A/2)[E_1[(\mu_a/\rho_a)h\rho_a] - \exp[(\alpha/\rho_s)h\rho_a(\mu_a/\rho_a)/(\mu_s/\rho_s)] \cdot$$

$$E_1[(\mu_a/\rho_a)h\rho_a + (\alpha/\rho_s)h\rho_a(\mu_a/\rho_a)/(\mu_s/\rho_s)]], \qquad (3.1.3.5)$$

where $E_1(t)$ is the exponential integral of the first order.

The case of the plane source distribution is obtained from the above by letting $\alpha/\rho_s \to \infty$. This yields for the differential angular flux:

$$\frac{d\phi}{d\theta} = (S_A/2)\tan\theta \exp[-(\mu_a/\rho_a)h\rho_a/\cos\theta], \qquad (3.1.3.6)$$

and the θ-integration gives:

$$\phi = (S_A/2)\ E_1[(\mu_a/\rho_a)h\rho_a] \ . \qquad (3.1.3.7)$$

The homogeneously distributed source is described for $\alpha/\rho_s=0$. Inserting this in equation (3.1.3.4) yields:

$$\frac{d\phi}{d\theta} = \frac{S_o \sin\theta\ \exp[-(\mu_a/\rho_a)h\rho_a/\cos\theta]}{2(\mu_s/\rho_s)\rho_s}, \qquad (3.1.3.8)$$

and for the total flux:

$$\phi = [(S_o/\rho_s)/(2\mu_s/\rho_s)]E_2[(\mu_a/\rho_a)h\rho_a], \qquad (3.1.3.9)$$

where $E_2(t)$ is the exponential integral of the second order. S_o is expressed in terms of activity per unit volume, which is converted to activity per unit weight, S, by division with the soil density giving:

$$\phi = [S/(2\mu_s/\rho_s)]\ E_2[(\mu_a/\rho_a)h\rho_a], \qquad (3.1.3.10)$$

and it is noted in this case that ϕ is independant of the soil density.

The calculations of ϕ/S and of ϕ/S_A are made using values for the mass attenuation coefficients from ref. 7. The values of μ_a/ρ_a apply to an air temperature of 20°C and a pressure of 760 mm Hg and the values of μ_s/ρ_s apply to a soil composition of 13.5% Al_2O_3, 4.5% Fe_2O_3, 67.5% SiO_2, 4.5% CO_2, and 10.0% H_2O. Furthermore, a soil density of 1.6 g/cm^3 is used.

The exponential integrals are calculated on a computer by means of numerical integration of the equations (3.1.3.4), (3.1.3.6) and (3.1.3.8) and the quantities computed with this technique prove identical to tabulated values of the integrals.

For the naturally occurring radionuclides with a uniform distribution in the soil, ϕ/S is shown versus energy in fig. 3.1.3.2. ϕ/S is here expressed in $\frac{\text{photons/cm}^2\text{/s}}{\text{photons/g/s}}$, which is converted to $\frac{\text{photons/cm}^2\text{/s}}{\text{pCi/g}}$ by multiplication with $0.037 \cdot f$, where f is the gamma yield for the gamma emitter in question.

Data on the ^{238}U and ^{232}Th series are taken from ref. 14. For ^{40}K, a gamma energy of 1460.8 keV and a gamma yield of 0.107 are used. The final values of ϕ/S for the prominent emission

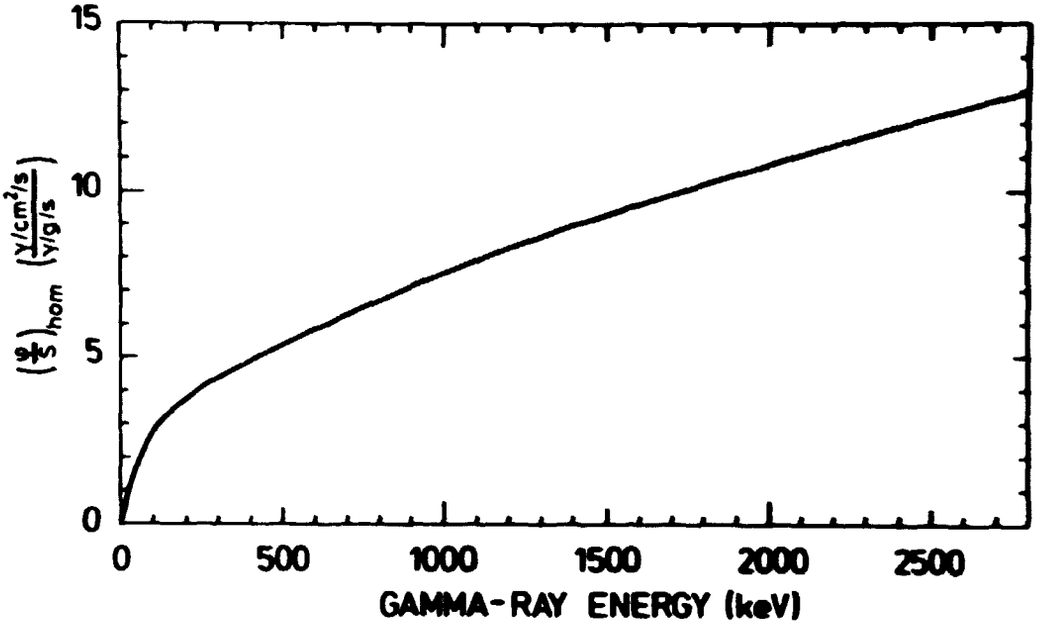

Fig. 3.1.3.2. Uncollided gamma flux (photons/cm^2/s) 1 m above ground per unit concentration (photons/g/s) of uniformly distributed sources in the soil as a function of gamma-ray energy (kev).

lines from the naturally occurring radionuclides are listed in table 4.1.3.1.

For fallout radionuclides, the only gamma-emitting isotope with a sufficiently long half-life to permit an exponential distribution in the soil is ^{137}Cs, and for this reason ϕ/S_A is calculated only for this isotope. Equation (3.1.3.5) yields ϕ/S_A in units of $\frac{\text{photons/cm}^2\text{/s}}{\text{photons/cm}^2\text{/s}}$ which is converted to $\frac{\text{photons/cm}^2\text{/s}}{\text{mCi/km}^2}$ by multiplication by $0.0037 \cdot f$. ϕ/S_A is shown in fig. 3.1.3.3 versus the depth distribution parameter α/ρ_s.

For surface-distributed fallout radionuclides, ϕ/S_A is calculated from equation (3.1.3.7) and the results are listed in table 3.1.4.2.

3.1.4. Uncollided Gamma Flux per Unit Exposure Rate

The uncollided gamma flux per unit exposure rate $\phi/\dot{X}$ is obtained from ϕ/S by division with $\dot{X}/S$.

The exposure rate per unit concentration of the source, $\dot{X}/S$, is calculated by solving the gamma-ray transport equation for the situation shown in fig. 3.1.3.1, which requires elaborate mathematical and computational techniques.

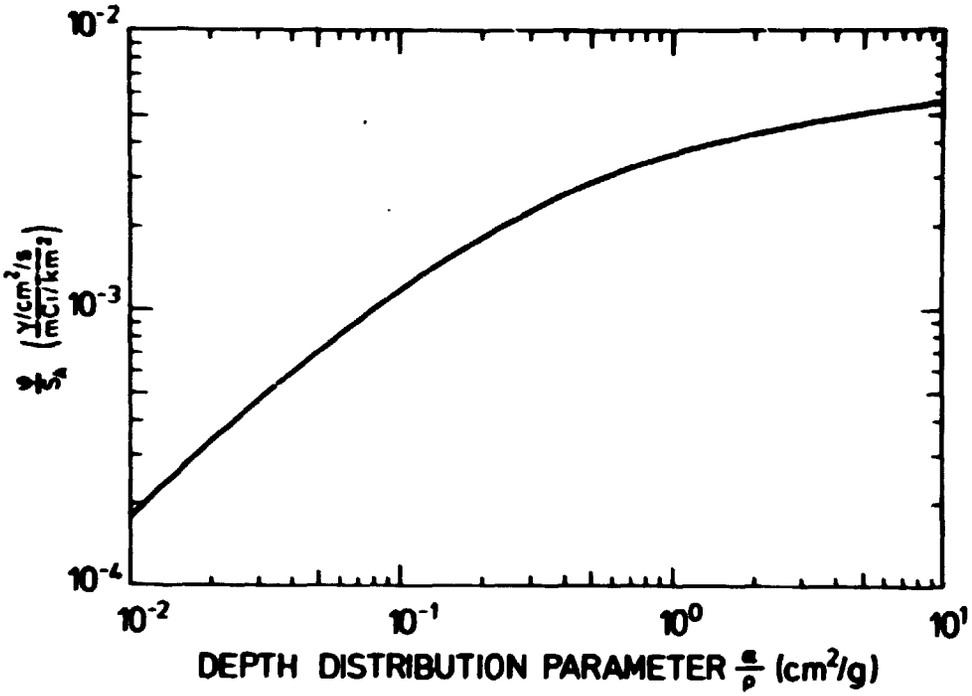

Fig. 3.1.3.3. Uncollided gamma flux (photons/cm²/s) 1 m above ground per unit concentration (mCi/km²) of ^{137}Cs exponentially distributed in the soil as a function of α/ρ (cm²/g).

The values of $\dot{X}/S$ for naturally occurring radionuclides with a uniform distribution are taken from ref. 15, and are listed in table 3.1.4.1.

Table 3.1.4.1

Exposure rate 1 m above ground per unit concentration of naturally occurring radionuclides

Nuclide	Concentration	Exposure rate
^{40}K	1%	1.52 μR/h
	1 pCi/g	0.103 μR/h
^{238}U series	1 ppm	0.63 μR/h
	1 pCi/g	1.89 μR/h
^{232}Th series	1 ppm	0.31 μR/h
	1 pCi/g	0.79 μR/h

Values of $\dot{X}/S_A$ for exponentially and surface-deposited fallout are taken from ref. 7. For ^{137}Cs, $\dot{X}/S_A$ versus α/ρ_s is shown in fig. 3.1.4.1. The values of $\dot{X}/S_A$ for surface-deposited fallout are listed in table 3.1.4.2.

3.1.5. Influence of Source Distribution

A major problem in the evaluation of field spectroscopic measurements is the determination of a proper relaxation length for exponentially distributed sources in the soil.

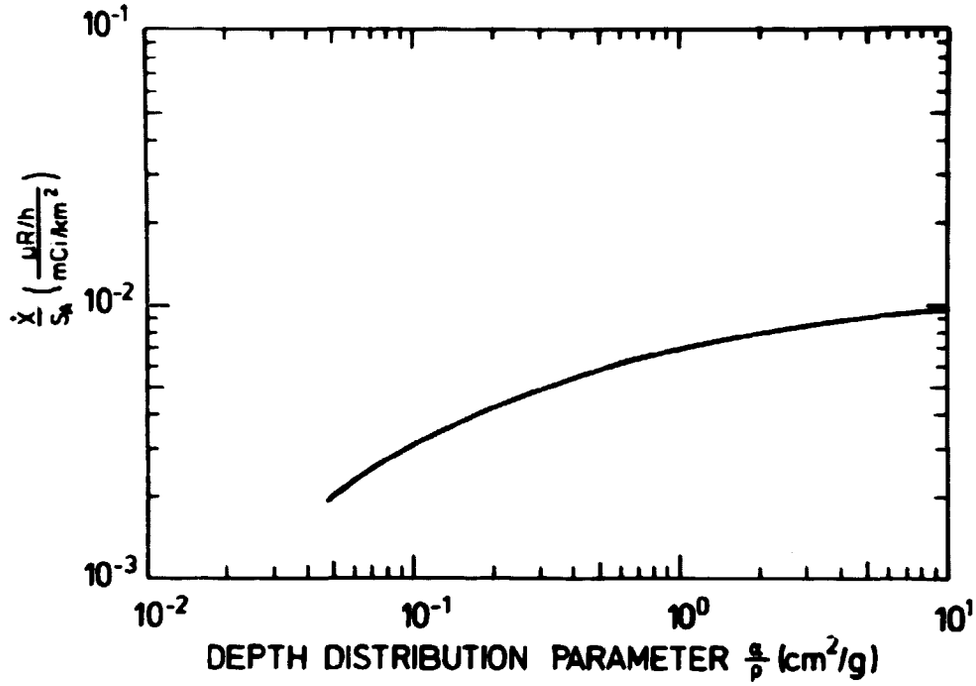

Fig. 3.1.4.1. Exposure rate (μR/h) 1 m above ground per unit concentration (mCi/km^2) of ^{137}Cs exponentially distributed in the soil as a function of α/ρ (cm^2/g).

Table 3.1.4.2

Data for surface-deposited fallout

Nuclide	Energy (keV)	Gamma yield (photons/disint.)	ϕ/S_A ($\frac{photons/cm^2/s}{mCi/km^2}$)	$\dot{X}/S_A$ ($\frac{\mu R/h}{mCi/km^2}$)
^{95}Zr	724.2	0.430	3.27 (-3)	1.35 (-2)
^{95}Zr	756.7	0.546	4.18 (-3)	-
^{95}Nb	765.8	0.990	7.58 (-3)	1.41 (-2)
^{103}Ru	496.9	0.900	6.59 (-3)	9.22 (-3)
^{125}Sb	176.3	0.063	4.17 (-4)	8.29 (-3)
^{125}Sb	428.0	0.296	2.13 (-3)	-
^{125}Sb	600.8	0.184	1.37 (-3)	-
^{131}I	364.5	0.824	5.84 (-3)	7.28 (-3)
^{137}Cs	661.6	0.846	6.38 (-3)	1.06 (-2)
^{140}Ba	162.9	0.062	4.06 (-4)	3.66 (-3)
^{140}Ba	537.4	0.238	1.77 (-3)	-
^{140}La	487.0	0.457	3.34 (-3)	3.96 (-2)
^{140}La	1596.2	0.960	7.98 (-3)	-
^{141}Ce	145.5	0.493	3.21 (-3)	1.31 (-3)
^{144}Ce	133.5	0.108	6.98 (-4)	3.27 (-4)

The importance of an accurate knowledge of the source distribution is illustrated in figs. 3.1.3.3 and 3.1.4.1 showing respectively, ϕ/S_A and $\dot{X}/S_A$ for ^{137}Cs. It is seen for ϕ/S_A that the uncertainty of α/ρ_s becomes of greater significance as the distribution approaches homogeneity ($\alpha/\rho_s \rightarrow 0$). This is also the case for $\dot{X}/S_A$, but to a somewhat lesser extent.

The true distribution can be inferred from laboratory measurements of collected soil samples, but the samples may not be representative, because of the very large area registered by the detector in a field measurement. From superficially deposited ^{137}Cs, 90% of the uncollided gamma flux 1 m above ground originates from distances within 60 m, corresponding to an area of 11300 m^2, while the distance for a uniform distribution decreases to 8 m corresponding to an area of 200 m^2 [11].

The ground roughness, which has not been included in the calculation model, tends to shield the detector from the radiating source in a field measurement. From the detector, the source seems to be buried more deeply in the soil than it really is. This effect can be taken into account by ascribing a greater relaxation length to the distribution than the true one. Another approach is to use the fact that ground roughness effects decrease with increasing height above ground. The latter approach was used for surface deposited fallout in ref. 16, where the ground roughness is expressed in terms of equivalent height of air. This fictitious height is added to the original height above the ground in the calculations and the resulting reduction factors give the reduction in the dose rate due to the additional height of air.

This method is applied in order to make a first approximation of the influence of ground roughness in field measurements of ^{137}Cs. The variations with height above ground of exposure rate and uncollided gamma flux from exponentially distributed ^{137}Cs [17] have provided the basis for reduction factors calculated for surface deposition and for deeper deposition. These are listed in table 3.1.5.1.

For a measurement in an ordinary plowed field, where ^{137}Cs is distributed exponentially with a depth distribution parameter of $\alpha/\rho_s = 0.1$ cm^2/g, a median value of the reduction factor for uncollided 662 keV photons is 0.74 and for the corresponding total exposure rate 0.85. This means that the ground roughness

Table 3.1.5.1

Factors describing the reduction of the uncollided gamma flux and exposure rate from fresh and aged fallout (^{137}Cs) due to various types of ground roughness

	Fictitious height m	Flux reduction $\frac{\alpha}{\rho} = \infty$	Flux reduction $\frac{\alpha}{\rho} = 0.1\ m^2/g$	Exposure rate reduction $\frac{\alpha}{\rho} = \infty$	Exposure rate reduction $\frac{\alpha}{\rho} = 0.1\ cm^2/g$
Smooth plane	0	1.00	1.00	1.00	1.00
Paved areas	0-1.5	1.00-0.78	1.00-0.94	1.00-0.83	1.00-0.97
Lawns	1.5-3	0.78-0.67	0.94-0.89	0.83-0.74	0.97-0.94
Gravelled areas	3-6	0.67-0.53	0.89-0.80	0.74-0.64	0.94-0.88
Ordinary plowed field	6-12	0.53-0.40	0.80-0.67	0.64-0.52	0.88-0.81
Deeply plowed field	12-18	0.40-0.34	0.67-0.58	0.52-0.46	0.81-0.75

causes a reduction of 26% of the uncollided gamma flux measured by the detector, and that the corresponding exposure rate is reduced by 15%.

With these reduction factors an overall value of α/ρ_s can be estimated. From fig. 3.1.3.3 it is seen that a 26% reduction of ϕ/S_A for $\alpha/\rho_s = 0.1\ cm^2/g$ corresponds to the value of ϕ/S_A for $\alpha/\rho_s = 0.067\ cm^2/g$, and from fig. 3.1.4.1 it follows that a 15% reduction of $\dot{X}/S_A$ for $\alpha/\rho_s = 0.1\ cm^2/g$ corresponds to a value of $\dot{X}/S_A$ for $\alpha/\rho_s = 0.072\ cm^2/g$. The average value of $\alpha/\rho_s = 0.07\ cm^2/g$ will thus describe the combination of the true distribution and the ground roughness. In other terms the ground roughness is described for this particular site by increasing the true relaxation length for the ^{137}Cs distribution by 40%.

3.1.6. Influence of ^{222}Rn in the Air

The calculational model shown in fig. 3.1.3.1 deals only with radioactive sources distributed in the ground. When estimating the content of ^{226}Ra in the soil from field measurements, an error is introduced because the presence of ^{222}Rn daughters in the air is neglected.

The principal gamma emitters in the ^{238}U series are ^{214}Pb and ^{214}Bi, which are among the short-lived daughter products of ^{222}Rn, the successor of ^{226}Ra (table 3.1.1). Since ^{222}Rn is a gas with a relatively long half-life, it may emanate in significant amounts from the upper layers of the soil into the atmosphere and travel over considerable distances with the wind. The emanation from the soil is governed by such factors as soil moisture, air temperature and barometric pressure, so the local ^{222}Rn concentrations in the air are critically de-

pendant on meteorological parameters. When airborne ^{222}Rn decays, the short-lived daughter products attach to aerosols and remain distributed in the air, where they contribute to the gamma flux from the daughter products contained in the ground. In a field measurement, the detector is naturally unable to distinguish between the two source distributions, but usually the airborne contribution is negligible[18]. A quantitative assessment of this contribution is made in a later section.

3.2. NaI(Tl) Spectrum Evaluation

The basis for the NaI(Tl) spectrum evaluation is a method described by Løvborg et al.[19] that is applicable for the in situ determination of the naturally occurring radionuclides, assuming secular equilibrium for the two decay series.

The gamma-ray intensities are recorded in three energy intervals centered at the 1.46 MeV emission line of ^{40}K, the 1.76 MeV emission line of ^{214}Bi from the ^{238}U series, and the 2.62 MeV emission line of ^{208}Tl from the ^{232}Th series.

The count rates N_K, N_U and N_{Th} in the three energy intervals are all linear combinations of the corresponding radionuclide concentrations C_K, C_U and C_{Th}, which is expressed in the following equation:

$$\begin{Bmatrix} N_K \\ N_U \\ N_{Th} \end{Bmatrix} = \begin{bmatrix} A_{11} & A_{12} & A_{13} \\ A_{21} & A_{22} & A_{23} \\ A_{31} & A_{32} & A_{33} \end{bmatrix} \begin{Bmatrix} C_K \\ C_U \\ C_{Th} \end{Bmatrix} \qquad (3.2.1)$$

The three diagonal elements A_{ii} describe the total absorption of the 1.46, 1.76 and 2.62 MeV gamma rays in the detector. The coefficient A_{12} describes the contribution to the energy interval at 1.46 MeV from the ^{238}U series, and the coefficients A_{13} and A_{23} describe the contribution from the ^{232}Th series to the energy intervals at 1.46 and 1.76 MeV, respectively. The coefficients A_{21} and A_{31} must be zero as they describe the contribution from ^{40}K to the energy intervals at 1.76 and 2.62 MeV, respectively. The coefficient A_{32}, describing the ^{238}U series contribution to the interval at 2.62 MeV, will be small due to the total absorption of a weak emission line of 2.45 MeV from ^{214}Bi.

With a knowledge of the proper matrix coefficients A_{ij}, the radionuclide concentrations are determined from a field measurement expressed in vector and matrix denomination:

$$\underline{C} = \underline{\underline{A}}^{-1} \underline{N} \ . \qquad (3.2.2)$$

The matrix coefficients are determined from calibration measurements made under circumstances similar to those for the field measurements, but where the radionuclide concentrations in the ground are known. Measurements at three locations where the individual radionuclide concentrations are linearly independant suffice for the determination. The three count rate vectors and the three concentration vectors, one for each location, constitute two matrices $\underline{\underline{N}}$ and $\underline{\underline{C}}$, respectively, which are related through the equation:

$$\underline{\underline{N}} = \underline{\underline{A}} \ \underline{\underline{C}} \ . \qquad (3.2.3)$$

For the unknown matrix this yields:

$$\underline{\underline{A}} = \underline{\underline{N}} \ \underline{\underline{C}}^{-1} . \qquad (3.2.4)$$

4. CALIBRATION

4.1. Calibration of Ge(Li) Detector System

4.1.1. Angular Correction Factor

The calculation of the correction factor N_f/N_o from equation (3.1.1.1) is based on the assumption that the response of the detector is cylinder-symmetric. The validity of this assumption was investigated from measurements performed by placing a multigamma source with 15^o intervals in a horizonal plane around the detector at a distance of 50 cm. The response for the gamma energies in the interval from 122 to 1408 keV showed no deviation from symmetry, so the assumption was accepted.

The angular response $R(\theta)$ was determined from measurements performed by placing point sources in a vertical plane under the detector at a distance of 1 m (fig. 4.1.1.1). An analytical expression for the angular variation for each energy was obtained from fitting a polynomial by means of the least squares

method to the results for the normalized count rates. The gamma energies of the point sources ranged from 60 to 1408 keV. Examples of R(θ) for 2 different energies are shown in fig. 4.1.1.2.

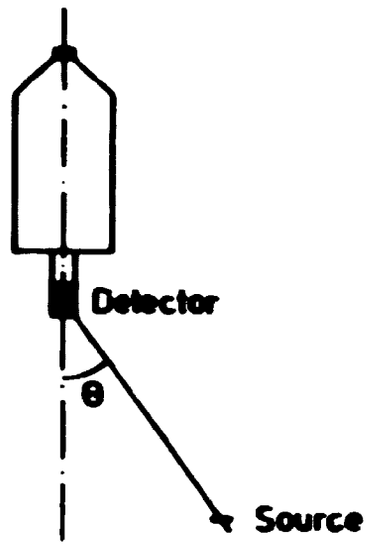

Fig. 4.1.1.1. Schematic set-up for the determination of the angular response of the Ge(Li) detector.

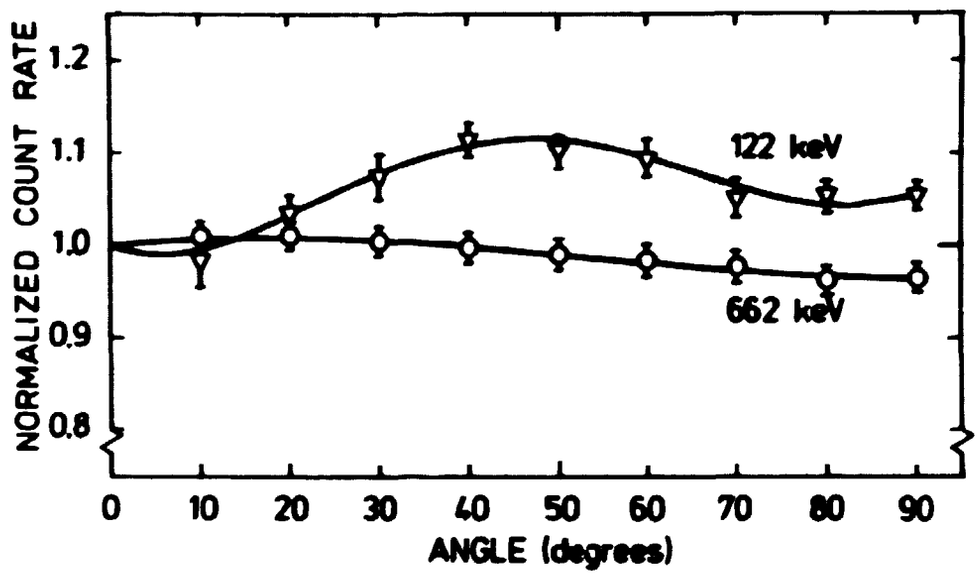

Fig. 4.1.1.2. Examples of angular response of Ge(Li) detector.

The response remains almost constant for gamma energies greater than 150 keV, while for lower energies variations occur because the low energy gamma rays are easily shielded and interact in the surface of the detector material.

N_f/N_o was calculated by numerical integration of equation (3.1.1.1) using the analytical expressions of $R(\theta)$ and the appropriate expressions of $d\phi/d\theta$ from section 3 according to the source distribution. Results of N_f/N_o versus energy for uniformly distributed sources are shown in fig. 4.1.1.3 and for surface deposited sources in fig. 4.1.1.4. The values of N_f/N_o for ^{137}Cs distributed uniformly and deposited on the surface are 0.98 and 0.97, respectively, which means that N_f/N_o for exponentially distributed ^{137}Cs in the soil can be considered as constant for all values of the distribution parameter α/ρ_s.

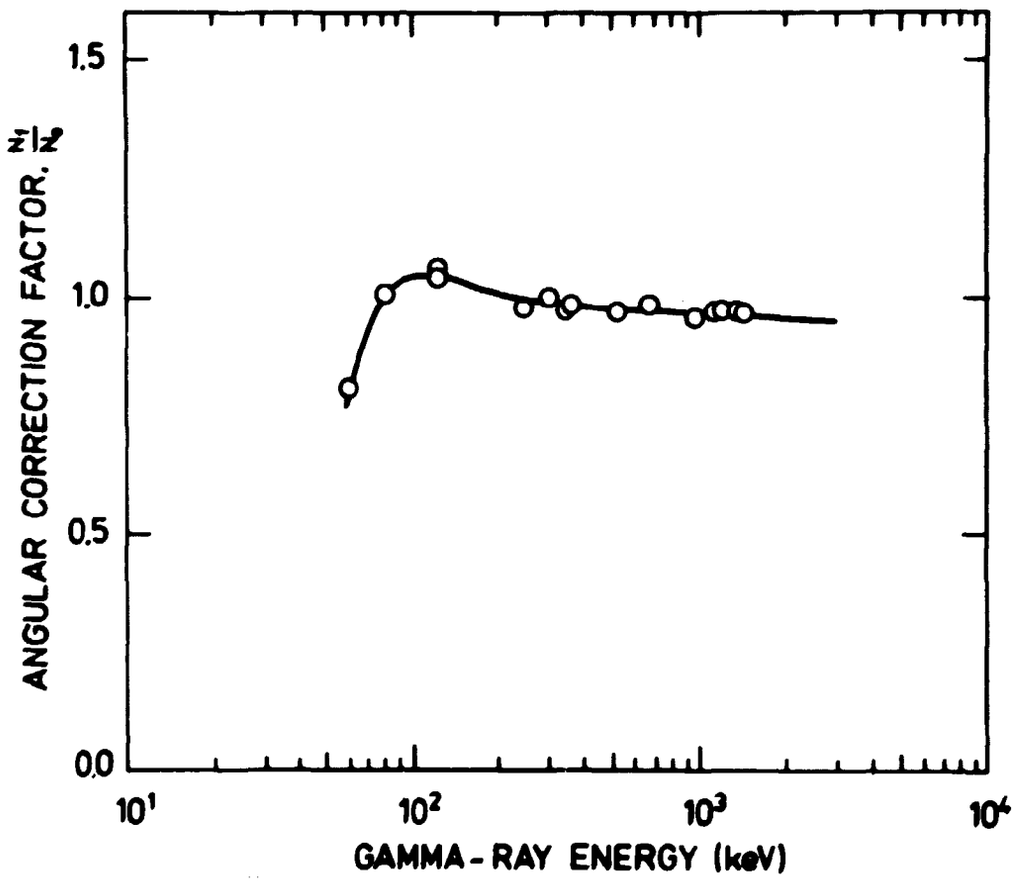

Fig. 4.1.1.3. Correction factor, N_f/N_o, for angular dependence of peak detection efficiency of Ge(Li) detector for uniformly distributed sources in the soil as a function of gamma-ray energy (kev).

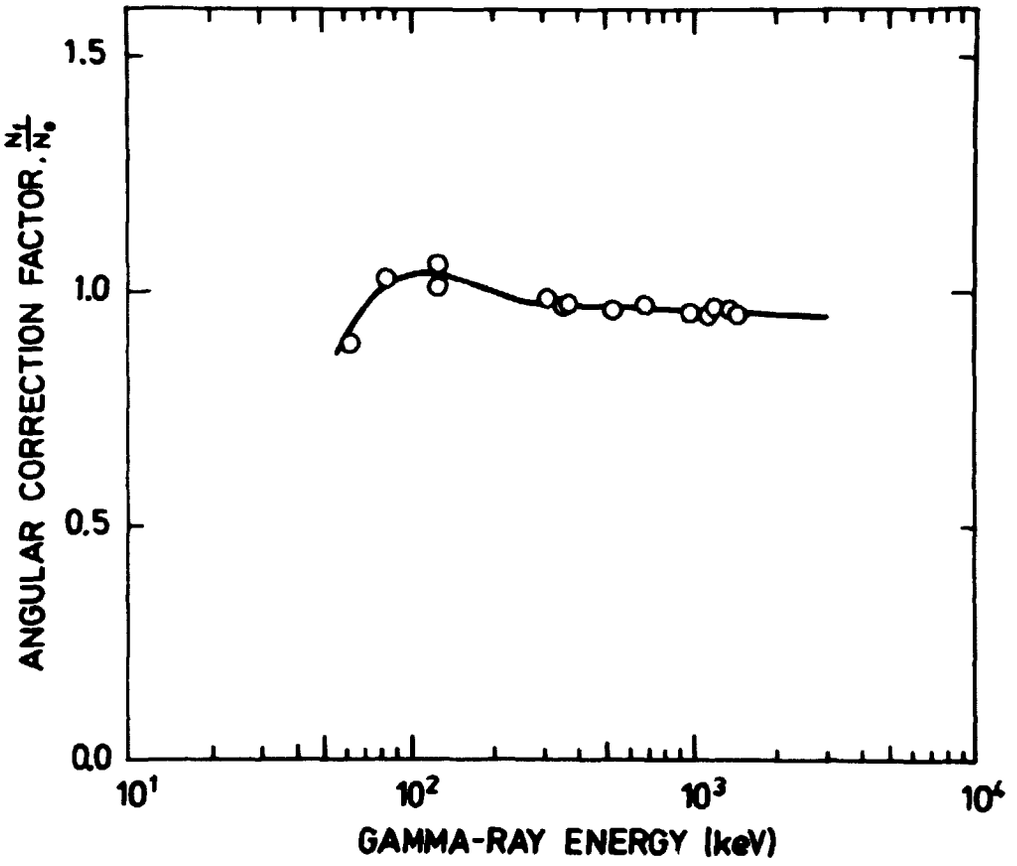

Fig. 4.1.1.4. Correction factor, N_f/N_o, for angular dependence of peak detection efficiency of Ge)Li) detector for surface deposited sources on the soil as a function of gamma-ray energy (keV).

4.1.2. Full Energy Peak Efficiency

As calibration sources were used ^{241}Am, ^{133}Ba, ^{57}Co, ^{22}Na, ^{137}Cs, ^{54}Mn, ^{60}Co and ^{152}Eu as primary standards and ^{226}Ra as a secondary standard. The sources were placed 1.5 m underneath the detector during the measurements. The resulting full energy peak efficiency N_o/ϕ is shown in fig. 4.1.2.1. For energies greater than 200 keV, the efficiency is calculated from the equation:

$$\ln(N_o/\phi) = 7.64 - 0.991 \ln(E) , \qquad (4.1.2.1)$$

where the energy E is expressed in keV.

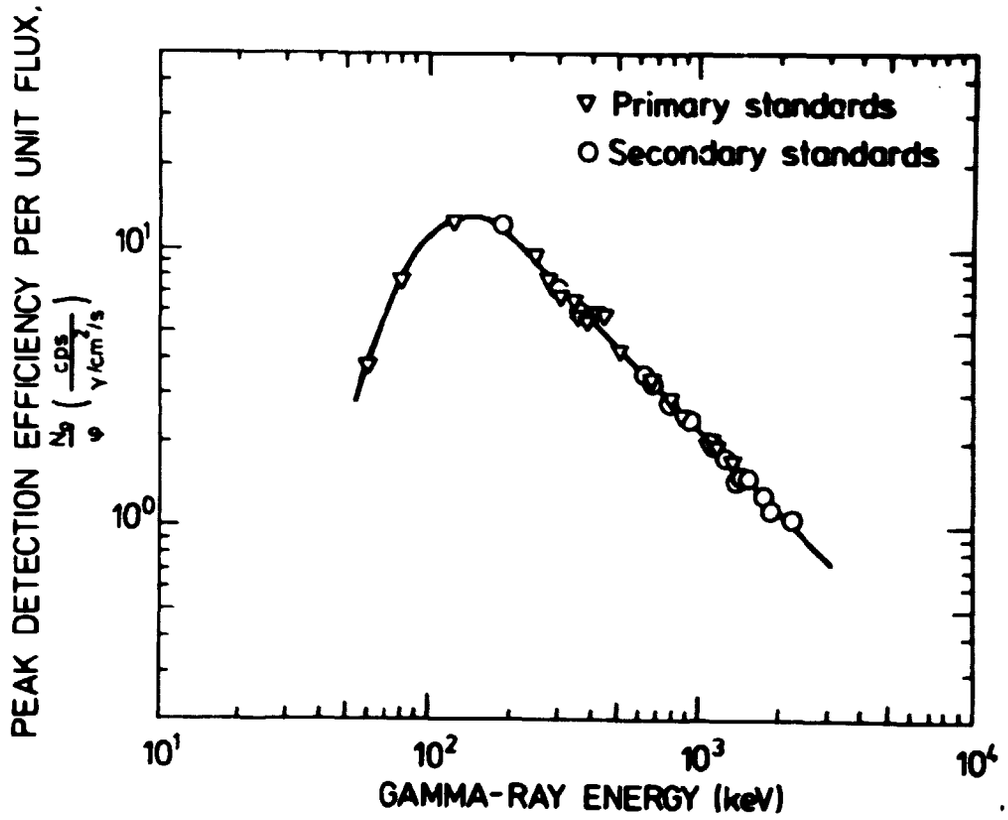

Fig. 4.1.2.1. Peak detection count rate (cps) of Ge(Li) detector per unit flux (photons/cm^2/s) as a function of gamma-ray energy (keV) measured at a source-detector distance of 1.5 m.

4.1.3. Presentation of Final Calibration Factors

The calibration factors N_f/S and $N_f/\dot{X}$ are listed in table 4.1.3.1 for the naturally occurring radionuclides. It must be noted that the values of N_f/S and $N_f/\dot{X}$ for the emission line of 186.1 keV from ^{226}Ra have been corrected for the fact that only 60% of the uncollided gamma flux of this energy in the environment originates from ^{226}Ra, the remaining 40% being due to a very close-lying emission line of 185.7 keV from the decay of ^{235}U[20].

For exponentially distributed ^{137}Cs, N_f/S_A and $N_f/\dot{X}$ are shown in figs. 4.1.3.1 and 4.1.3.2, respectively.

For surface-deposited fallout, the calibration factors are listed in table 4.1.3.2.

Table 6.1.3.1

Calibration factors for naturally occurring radionuclides

Nuclide	Energy (keV)	N_f/N_o	N_o/ϕ $(\frac{counts/s}{\gamma/cm^2/s})$	ϕ/S $(\frac{\gamma/cm^2/s}{pCi/g})$	N_f/S $(\frac{counts/s}{pCi/g})$	$N_f/\dot{H}$ $(\frac{counts/s}{\mu R/h})$
^{40}K	1460.8	0.961	1.51	3.62(-2)	5.25(-2)	2.87(-1)
^{238}U Series						
^{226}Ra	186.1	1.017	11.6	6.56(-3)	8.93(-2)	4.72(-2)
^{214}Pb	241.9	0.996	8.99	1.04(-2)	9.31(-2)	4.93(-2)
-	295.2	0.987	7.38	2.86(-2)	2.00(-1)	1.10(-1)
-	352.0	0.984	6.20	6.00(-2)	3.66(-1)	1.94(-1)
^{214}Bi	609.4	0.975	3.60	9.38(-2)	3.29(-1)	1.74(-1)
-	665.6	0.974	3.30	3.41(-3)	1.10(-2)	5.80(-3)
-	768.4	0.972	2.86	1.17(-2)	3.25(-2)	1.72(-2)
-	936.1	0.968	2.36	8.32(-3)	1.90(-2)	1.01(-2)
-	1120.4	0.965	1.97	4.27(-2)	8.12(-2)	4.29(-2)
-	1238.2	0.964	1.78	1.74(-2)	2.99(-2)	1.58(-2)
-	1377.8	0.962	1.60	1.51(-2)	2.32(-2)	1.23(-2)
-	1401.7	0.962	1.58	4.63(-3)	7.04(-3)	3.72(-3)
-	1408.0	0.962	1.57	7.96(-3)	1.25(-2)	6.61(-3)
-	1509.5	0.961	1.46	7.22(-3)	1.01(-2)	5.36(-3)
-	1729.9	0.958	1.28	1.04(-2)	1.28(-2)	6.75(-3)
-	1764.6	0.958	1.25	5.49(-2)	6.57(-2)	3.48(-2)
-	1847.7	0.957	1.20	8.04(-3)	9.23(-3)	4.89(-3)
-	2204.5	0.954	1.01	1.90(-2)	1.91(-2)	1.01(-2)
-	2448.0	0.953	0.907	6.66(-3)	5.76(-3)	3.05(-3)
^{232}Th Series						
^{228}Ac	129.1	1.048	12.7	2.85(-3)	3.79(-2)	1.36(-2)
-	209.5	1.005	10.4	5.74(-3)	6.00(-2)	2.15(-2)
^{212}Pb	238.6	0.995	9.12	6.63(-2)	6.02(-1)	2.16(-1)
^{224}Ra	241.0	0.995	9.0[illegible]	5.91(-3)	5.31(-2)	1.90(-2)
^{228}Ac	270.2	0.990	8.06	5.07(-3)	4.68(-2)	1.68(-2)
^{208}Tl	277.2	0.990	7.86	3.74(-3)	2.91(-2)	1.04(-2)
^{212}Pb	300.6	0.987	7.25	5.47(-3)	3.91(-2)	1.40(-2)
^{228}Ac	328.0	0.985	6.65	5.50(-3)	3.60(-2)	1.29(-2)
-	338.5	0.985	6.45	2.06(-2)	1.32(-1)	4.74(-2)
-	463.0	0.980	4.73	9.05(-3)	4.20(-2)	1.50(-2)
^{208}Tl	583.1	0.976	3.76	6.41(-2)	2.35(-1)	8.43(-2)
^{212}Bi	727.1	0.973	3.02	1.66(-2)	4.88(-2)	1.75(-2)
^{228}Ac	794.9	0.971	2.77	1.21(-2)	3.25(-2)	1.17(-2)
^{208}Tl	860.1	0.970	2.56	1.21(-2)	3.00(-2)	1.08(-2)
^{228}Ac	911.1	0.969	2.42	7.69(-2)	1.80(-1)	6.46(-2)
-	964.5	0.968	2.28	1.53(-2)	3.38(-2)	1.21(-2)
-	968.9	0.968	2.27	4.95(-2)	1.09(-1)	3.90(-2)
-	1588.1	0.960	1.39	1.63(-2)	2.18(-2)	7.80(-3)
^{208}Tl	2614.5	0.952	0.894	1.65(-1)	1.40(-1)	5.03(-2)

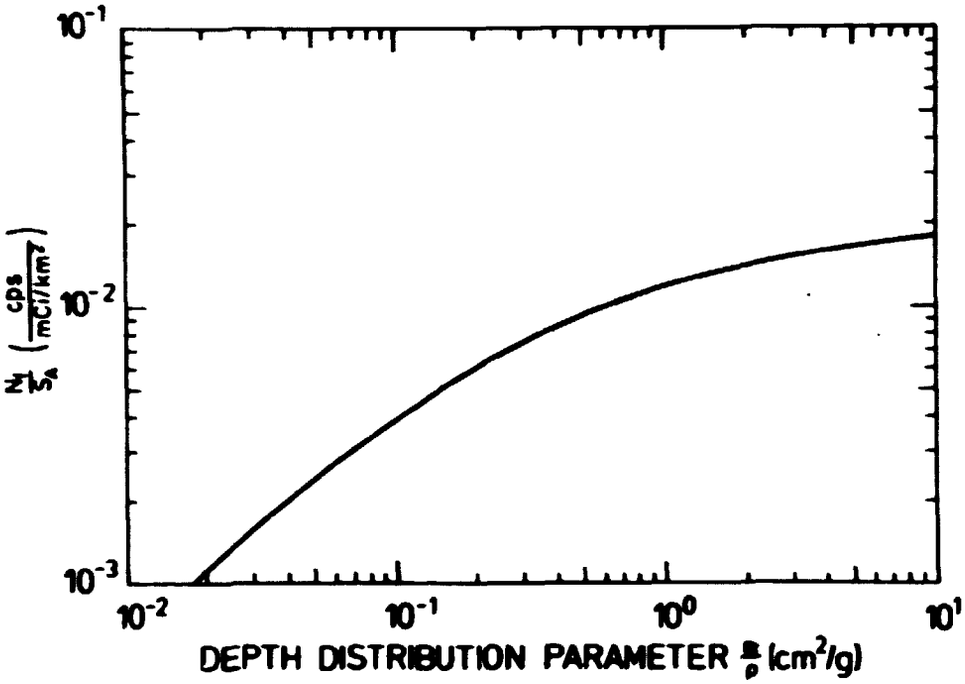

Fig. 4.1.3.1. Full energy peak count rate (cps) 1 m above ground per unit concentration (mCi/km^2) of ^{137}Cs exponentially distributed in the soil as a function of α/ρ (cm^2/g).

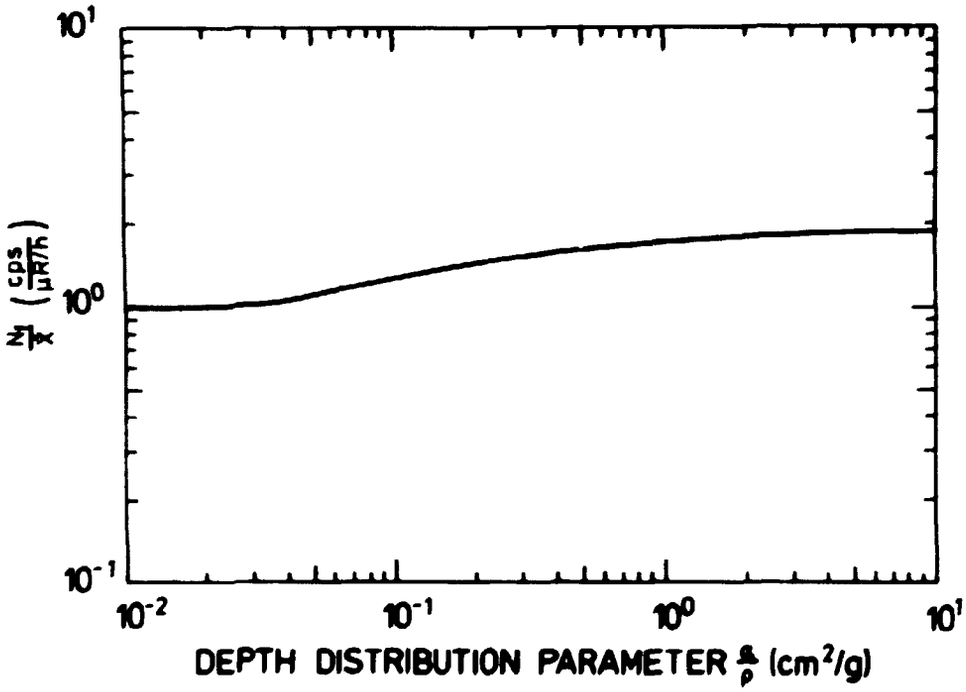

Fig. 4.1.3.2. Full energy peak count rate (cps) 1 m above ground per unit exposure rate (μR/h) from ^{137}Cs exponentially distributed in the soil as a function of α/ρ (cm^2/g).

Table 4.1.3.2

Calibration factors for surface-deposited fallout

Nuclide	Energy (keV)	N_f/N_o	N_o/ϕ (counts/s / photons/cm²/s)	ϕ/S_A (photons/cm²/s / mCi/km²)	N_f/S_A (counts/s / mCi/km²)	$N_f/\dot{X}$ (counts/s / μR/h)
^{95}Zr	724.2	0.965	3.03	3.27(-3)	9.56(-3)	7.08(-1)
^{95}Zr	756.7	0.964	2.90	4.18(-3)	1.17(-2)	8.67(-1)
^{95}Nb	765.8	0.964	2.87	7.58(-3)	2.10(-2)	1.49 (0)
^{103}Ru	496.9	0.969	4.41	6.59(-3)	2.82(-2)	3.06 (0)
^{125}Sb	176.3	0.995	12.3	4.17(-4)	5.10(-3)	6.15(-1)
^{125}Sb	428.0	0.971	5.11	2.13(-3)	1.06(-2)	1.28 (0)
^{125}Sb	600.8	0.967	3.65	1.37(-3)	4.84(-3)	5.84(-1)
^{131}I	364.5	0.973	5.99	5.84(-3)	3.40(-2)	4.67 (0)
^{137}Cs	661.6	0.966	3.32	6.38(-3)	2.05(-2)	1.93 (0)
^{140}Ba	162.9	1.000	12.7	4.06(-4)	5.16(-3)	1.41 (0)
^{140}Ba	537.4	0.968	4.08	1.77(-3)	6.99(-3)	1.91 (0)
^{140}La	487.0	0.969	4.49	3.34(-3)	1.45(-2)	3.66(-1)
^{140}La	1596.2	0.955	1.39	7.98(-3)	1.06(-2)	2.68(-1)
^{141}Ce	145.5	1.016	12.9	3.21(-3)	4.21(-2)	3.21 (1)
^{144}Ce	133.5	1.027	12.8	6.98(-4)	9.18(-3)	2.81 (1)

4.1.4. Measurements of Mass Attenuation Coefficients for Soil

The value of μ_s/ρ_s used for the calculations of ϕ/S and ϕ/S_A in section 3.1.3, and for the gamma-ray transport calculations yielding exposure rate data, is based on the soil composition previously mentioned. To get an impression of the comparability of these values with those of typical Danish soils, an experimental determination of μ_s/ρ_s was made on soil from two different locations near the laboratory. Samples were taken from the surface of the soil at both locations. The soil was cultivated at location 1 and had a density of 1.68 g/cm^3 ± 0.05 (1 S.E.) determined from 5 samples, while the soil at location 2 was uncultivated and had a high content of clay and a density of 1.78 g/cm^3 ± 0.05 (1 S.E.) determined from 5 samples. The gamma-ray attenuation was determined from two samples from each location using a multi-gamma source, and the results are shown in fig. 4.1.4.1.

It is noted that the experimental values of μ_s/ρ_s agree well with the values from ref. 7 used in the calculations, indicating the general applicability of the model soil composition to Danish soils. It is also seen that the experimental values of

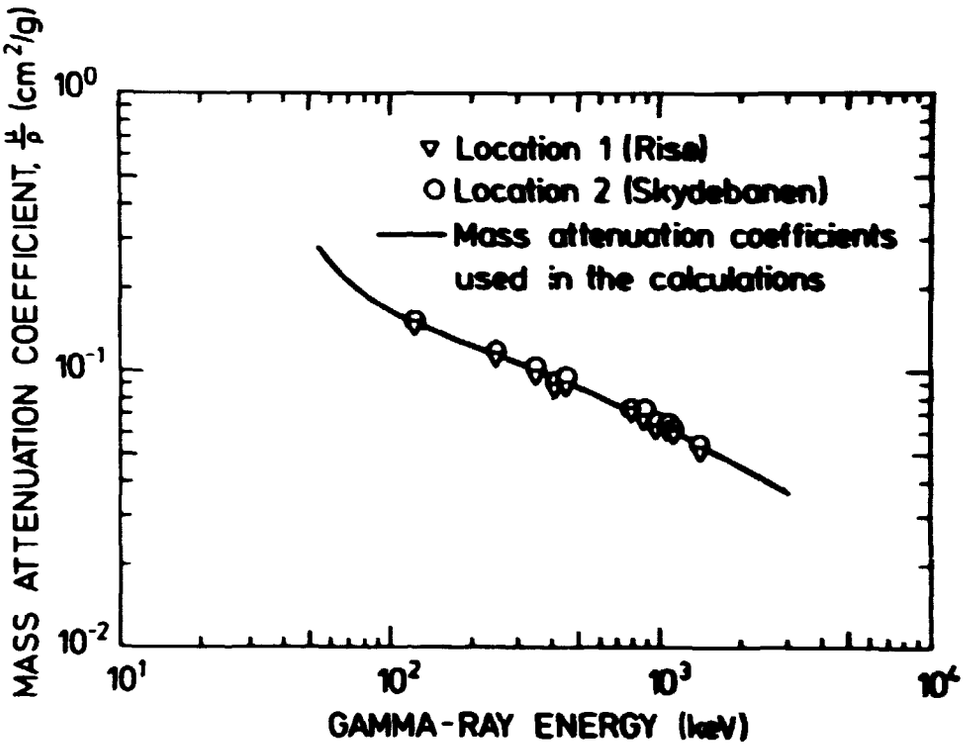

Fig. 4.1.4.1. Results of experimentally determined mass attenuation coefficients (cm^2/g) for soil samples as a function of gamma-ray energy. For comparison are shown the mass attenuation coefficients from ref. (7) used in the calculations.

μ_s/ρ_s for location 2 are a little higher than those for location 1. This is explained by the fact that soil from location 2 has a higher average atomic number than soil from location 1 because of the high content of clay minerals. These also cause the soil density to be greater at location 2 than at location 1.

4.2. Calibration of the NaI(Tl) Detector System

4.2.1. Measurements on Calibration Pads

The NaI(Tl) detector system was calibrated by means of measurements performed in approximated 2π-geometries over four concrete calibration pads. The pads are 3 m in diameter and 0.5 m thick and are numbered from 0 to 3. Pad 0 serves as a zero reference, pad 1 is enriched in potassium, pad 2 in thorium and pad 3 in uranium. Detailed descriptions of the pads are given in refs. 19 and 21.

The radionuclide concentrations of the pads are known from analyses of samples taken from the concrete mixtures when the pads were cast.

The gamma radiation from pad 3 is subject to seasonal variations of ± 20%, probably due to the migration of ^{222}Rn, but an apparent concentration of ^{238}U can be ascribed to the pad by employing a simple scintillometer method[21]. The radionuclide concentrations of the pads on the day of calibration are shown in table 4.2.1.1.

Table 4.2.1.2

Count rates (cps) recorded above the calibration pads with the NaI(Tl) detector

Energy interval	Pad 0	Pad 1	Pad 1	Pad 3
1330-1610 keV	3.95	26.21	72.86	26.25
1640-1910 keV	0.696	1.523	56.73	17.85
2440-2780 keV	0.393	0.622	2.348	17.49

The detector was placed with its center 8 cm above the surface of the pads while the calibration spectra were accumulated. From these, the gamma-ray intensities of the three radionuclides were excerpted in terms of counts per second in the energy intervals previously mentioned. The spectrum calculations were made by means of the computer program STATDATA[22]. The results are listed in table 4.2.1.2.

Table 4.2.1.1

Radionuclide concentrations of the calibration pads

Pad	% K	ppm U	ppm Th
0	1.0	0.8	2.4
1	7.0	4.2	2.7
2	0.8	6.3	151
3	1.0	179	8

4.2.2. Calculation of Calibration Matrix Coefficients

The calibration matrix coefficients are calculated from equation (3.2.4) with a few corrections due to differences between the calibration situation and the field measurement situation.

Because of the inevitable influence of the surroundings during the calibration measurements, unknown amounts of environmental radiation are included in the recorded count rates in table 4.2.1.2. As these contributions are presumably identical for each of the pads, their influence is eliminated by subtracting the recorded count rates from pad 0 from those of the other pads.

The corrections needed because of the finite size of the pads and the differences in detector height above source and source composition are approximated with corrections calculated for uncollided fluxes. The finite size of the pads is accounted for by increasing the count rates recorded in the energy intervals centered at 1461 and 1765 keV with 5.5% and those centered at 2615 keV with 6.5%[17]. As seen from equation (3.1.3.10), the remaining corrections amount to a multiplicative factor of $\frac{E_2[(\mu_a/\rho_a)h_f\rho_a]/(\mu_f/\rho_f)}{E_2[(\mu_a/\rho_a)h_c\rho_a]/(\mu_c/\rho_c)}$, where the indices f and c refer to field and calibration situations, respectively. The resulting factors are 0.965, 0.968 and 0.975 for the three energy intervals listed in order of increasing energy.

The calibration matrix coefficients are calculated using the data from tables 4.2.1.1 and 4.2.1.2 and the above-mentioned corrections by inserting the matrices $\underline{N}$ and $\underline{C}$ in equation (3.2.4), where

$$\underline{N} = \begin{Bmatrix} 20.6 & 70.2 & 22.7 \\ 0.847 & 55.2 & 17.5 \\ 0.030 & 2.03 & 17.8 \end{Bmatrix} , \qquad (4.2.2.1)$$

and

$$\underline{C} = \begin{Bmatrix} 6.0 & 0.0 & -0.2 \\ 3.4 & 178 & 5.5 \\ 0.3 & 5.6 & 149 \end{Bmatrix} . \qquad (4.2.2.2)$$

This yields for the calibration matrix:

$$\underline{A} = \begin{Bmatrix} 3.21 & 0.39 & 0.14 \\ -0.04 & 0.31 & 0.11 \\ -0.01 & 0.01 & 0.12 \end{Bmatrix} . \qquad (4.2.2.3)$$

It is noted that the coefficients A_{21}, A_{31} and A_{32} are small compared with the other coefficients, in agreement with the discussion in section 3.2. However, it is unphysical that A_{21} and A_{31} are negative. While the negative value of A_{31} can be ascribed to the uncertainty in the coefficient determination, the numerical value of A_{21} seems too large for this explanation. This matter will be referred to later.

The final calibration constants are obtained by inverting the matrix $\underline{A}$ and changing the units of the concentrations using the conversion factors 0.120% K per pCi/g of ^{40}K, 3.00 ppm ^{238}U per pCi/g, and 9.09 ppm ^{232}Th per pCi/g. This yields for equation (3.2.2):

$$\begin{Bmatrix} C_K \\ C_U \\ C_{Th} \end{Bmatrix} = \begin{bmatrix} 2.55 & -3.24 & -0.17 \\ 0.01 & 1.10 & -0.99 \\ 0.00 & -0.03 & 0.95 \end{bmatrix} \begin{Bmatrix} N_K \\ N_U \\ N_{Th} \end{Bmatrix}, \qquad (4.2.2.4)$$

where C_K, C_U and C_{Th} are in units of pCi/g, and N_K, N_U and N_{Th} in units of cps.

4.3. Calibration of Total Count Scintillometer

As the high-pressure ionization chamber mentioned in section 2.5 was not available during all the planned field measurements, the NaI(Tl) detector system was calibrated with reference to measurements of exposure rate in the air.

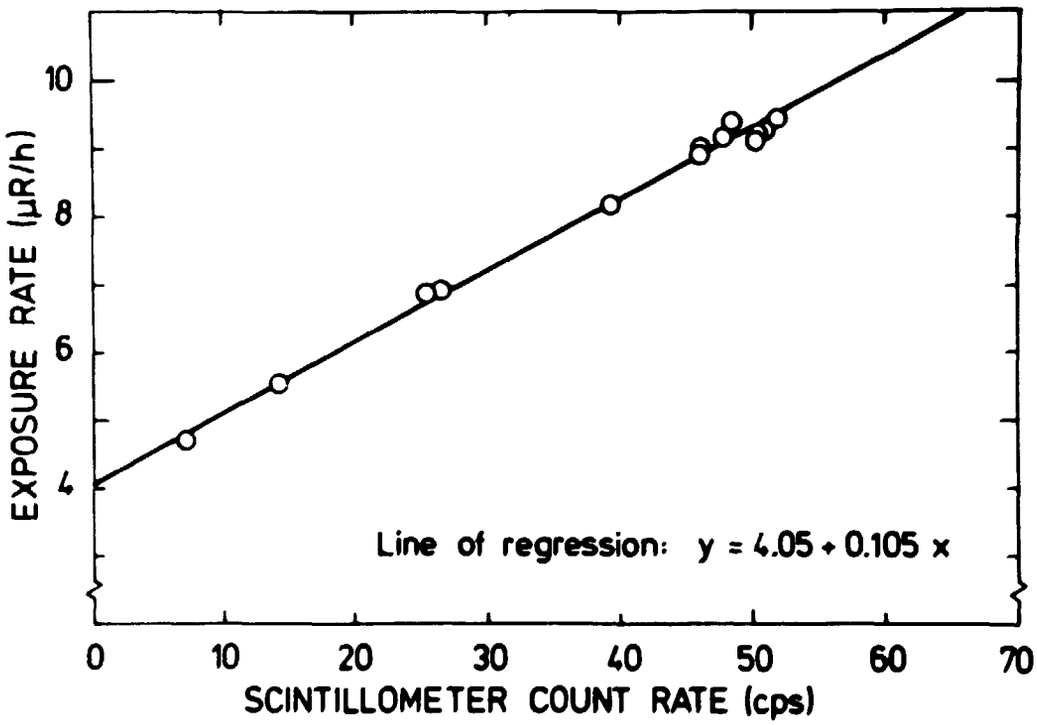

Fig. 4.3.1. Calibration of a 7.5 x 7.5 cm NaI(Tl) detector used as a total-count scintillometer with a counting threshold of 0.44 MeV. The exposure rate in air (μR/h) measured with a high pressure ionization chamber is depicted as a function of the scintillometer count rate (cps).

It has been demonstrated that the total count rate for a NaI(Tl) detector registering the radiation from uniformly distributed, naturally occurring radionuclides in a 2π-geometry, using a counting threshold of about 0.4 MeV, is proportional to the exposure rate in air at the point of detection[15]. Simultaneous measurements with the NaI(Tl) detector and the high-pressure ionization chamber at a number of locations provided the basis for the calibration. The result is shown in fig. 4.3.1.

The regression line has a zero intercept of 4.05 ± 0.22 μR/h and a slope of 0.105 ± 0.005 μR/h per cps, where the uncertainties stated are 95% confidence intervals. The interpretation of the intercept will be commented upon later.

5. COMPUTER ANALYSIS OF GE(LI) GAMMA-RAY SPECTRA

In the following a description is given of the computer program ANSP that processes gamma-ray spectra from Ge(Li) detectors. The program was designed to evaluate gamma-ray spectra from the field measurements, and thus special care had to be taken as these spectra are characterized by relatively poor counting statistics.

The program has been coded in ALGOL and adapted to the Risø B6700 computer. The spectra are available on punched paper

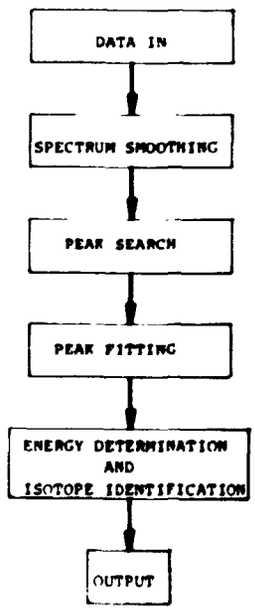

Fig. 5.1. Flow chart for main program ANSP.

tape and are read into the computer, whereafter the analysis is conducted from a remote terminal.

The analysis is outlined in fig. 5.1 and proceeds as follows:

1) A smoothing procedure is performed on the spectrum.

2) The spectrum is searched for peaks by checking whether the second derivative of the spectrum is numerically greater than its standard deviation. If this is the case, the area of the matching peak is calculated by using the total peak area method[23], and the peak area and the peak position are stored provided that the area is greater than a certain fraction of its standard deviation.

3) After finding the peaks in the spectrum, a Gaussian function is fitted to the data in an interval for each peak by employing a non-linear least squares method. If the fitting is successful, the area of each peak is calculated from the parameter values of the Gaussian function. If the fitting is unsuccessful, the area calculated with the total peak area method is retained.

4) The peak positions are converted to gamma-ray energies. The relationship between channel number and energy is determined from the positions of the most prominent peaks in the spectrum from the naturally occurring radionuclides.

5) The energies from the peaks are compared to gamma-ray energies from certain isotopes, and in the case of identification a final calculation and a print-out are performed. The isotopes include the naturally occurring radionuclides (table 4.1.3.1) and fallout isotopes (table 4.1.3.2).

6) Finally the spectrum is plotted. All the peaks found by the program are marked, and the identified peaks are supplied with gamma-ray energy and isotope designation.

5.1. Smoothing of Data

The spectra are smoothed using a moving average[24]. A polynomial of degree n is fitted by the least squares method to the data consisting of 2m+1 channels and the content of the center channel is replaced by the value of the polynomial in this channel. The value of the polynomial in the center channel is calculated according to

$$sms_i = \frac{1}{N} \sum_{j=-m}^{m} a_j y_{i+j} \quad , \qquad (5.1.1)$$

where y_{i+j} is the content of channel i+j, N and a_{-m}, ... , a_m are constants depending on n and m, and sms_i is the smoothed value in channel i. The choice of n and m depends on the detector resolution, which is fundamental for the width of the peaks in the spectrum. The choice constitutes a compromise between smoothing the statistical variation as far as possible while distorting the shape of the peaks as little as possible. This has been discussed elsewhere[25-27], and it is recommended to use 1-2 channels less in the smoothing process than used for the resolution of the detector (fwhm). Here we choose to use a five-point smoothing (m=2) and a second-degree polynomial, which yields for the polynomial coefficients:

$$sms_i = \frac{1}{35} (-3y_{i-2} + 12y_{i-1} + 17y_i + 12y_{i+1} - 3y_{i+2}). \qquad (5.1.2)$$

5.2. Peak Search

The peak search procedure is shown in fig. 5.2.1.

The peaks are characterized by significantly great negative values of the second derivative of the spectrum[28].

The statistical variation is reduced by calculating the second derivative of the smoothed spectrum. This is done directly from the original spectrum[24]

$$sds_i = \frac{1}{7} (2y_{i-2} - y_{i-1} - 2y_i - y_{i+1} + 2y_{i+2}), \qquad (5.2.1)$$

where sds_i is the smoothed second derivative for channel i.

In order to find the negative values of the second derivative, it is tested if

$$sds_i < 0, \text{ and } sds_{i-1} > sds_i, \text{ and } sds_{i+1} > sds_i. \qquad (5.2.2.)$$

When this condition is fulfilled, it is tested if the second derivative is numerically greater than its standard deviation

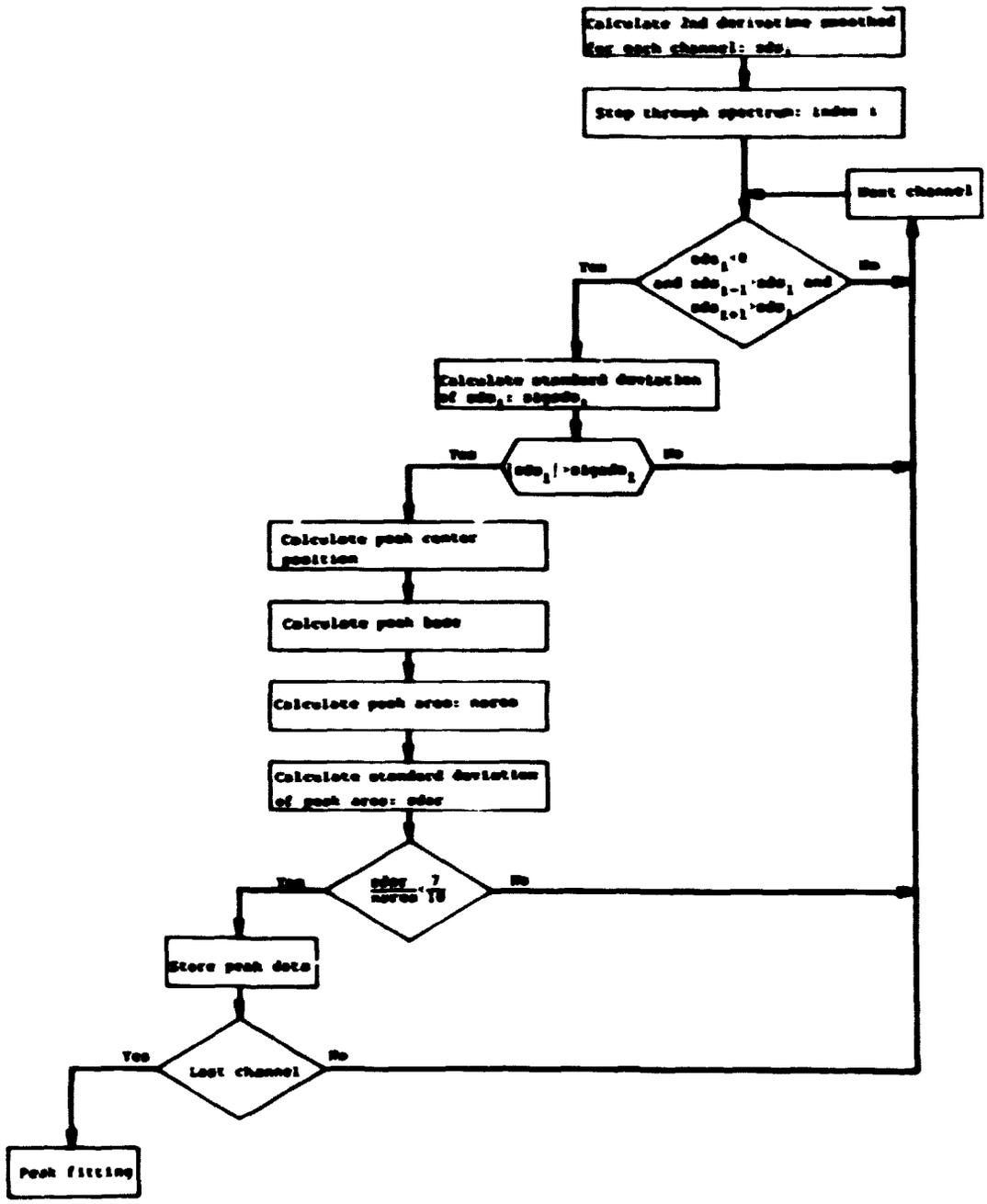

Fig. 5.2.1. Flow chart for peak search.

$$|sds_i| > sigsds_i, \qquad (5.2.3)$$

where

$$sigsds_i = \frac{1}{7}(4y_{i-2} + y_{i-1} + 4y_i + y_{i+1} + 4y_{i+2})^{\frac{1}{2}}. \qquad (5.2.4)$$

If this condition also holds, the area of the peak is calculated by the total peak area method.

First, the exact peak position is determined by fitting a Gaussian function to the five center channels of the peak. It is here assumed that the peak is described by a Gaussian function:

$$y = A \exp(ax^2 + bx + c). \qquad (5.2.5)$$

The function is transformed to a parabola:

$$\ln(y) = K(ax^2 + bx + c) , \qquad (5.2.6)$$

and b and 2a are calculated as the first and the second derivative, respectively, in the center channel x_o of the parabola that approximates the five data points by a least squares fit[24]:

$$b = \frac{1}{10}[-2 \ln(y_{-2}) - \ln(y_{-1}) + \ln(y_1) + 2 \ln(y_2)] \qquad (5.2.7)$$

and

$$2a = \frac{1}{7}[2 \ln(y_{-2}) - \ln(y_{-1}) - 2 \ln(y_o) - \ln(y_1) + 2 \ln(y_2)]. \qquad (5.2.8)$$

The peak position x_p is calculated as

$$x_p = x_o - \frac{b}{2a} , \qquad (5.2.9)$$

and this value corresponds closely to the value determined by the non-linear least squares fit described in the following section.

The transition from peak to background is found by determining the channel h where

$$sms_{h+1} < sms_h - \sqrt{sms_h} \quad \text{or} \quad sms_{h+2} < sms_h - \sqrt{sms_h} \tag{5.2.10}$$

from the right, and the channel v where

$$sms_{v-1} < sms_v - \sqrt{sms_v} \quad \text{or} \quad sms_{v-2} < sms_v - \sqrt{sms_v} \tag{5.2.11}$$

from the left[28]. The two channels h and v determine the background under the peak, and the area A is calculated as

$$A = \sum_{i=v+1}^{r-1} sms_i - (h-v-1)\,\frac{sms_v + sms_h}{2} \,. \tag{5.2.12}$$

The standard deviation of the area is

$$\Delta A = \left\{ \sum_{i=v+1}^{r-1} sms_i + (h-v-1)^2\,\frac{sms_v + sms_h}{4} \right\}^{\frac{1}{2}} . \tag{5.2.13}$$

Peaks with a relative standard deviation greater than 70% are rejected. The areas and positions of all accepted peaks are stored.

There are three reasons for involving area computation in the peak search:

1) It has shown that spurious peaks are effectively eliminated hereby.

2) If the fitting procedure should fail for a certain peak, the remaining computations are made with the area already determined.

3) The computations involved are not very time-consuming.

5.3. Peak Fitting

5.3.1. General Remarks

Peak fitting is included in the spectrum analysis because of the shortcomings of the total peak area method. This method implies poor reproducibility in repeated identical measurements in the case of poor counting statistics. The way in which the

peak base is determined is based upon the variation of the channel content from channel to channel, see equations (5.2.10) and (5.2.11). The peak is analyzed through a very narrow window of 3 channels only, and in the case of poor counting statistics, the identification of the transition between peak and background is often poor. This narrow window also makes it difficult to detect close-lying peaks, and if two peaks are so close that there is no minimum between them, they will not be discernable.

Unlike the total peak area method, peak fitting is characterized by a broad window using a fitting interval of about 20 channels. In this case poor counting statistics will not be critical for the fit, but will, of course, contribute to reduce the goodness of the fit.

5.3.2. Method of Fitting

This section outlines the method of non-linear least squares fitting used in ANSP[29].

It is assumed that the data consist of m observations $[(x_i, y_i)w_i]_{i=1}^{m}$, where x_i is the i^{th} channel in the fitting interval, y_i the corresponding channel content, and w_i the corresponding weight. Statistical weighing is used and thus $w_i = (y_i)^{-\frac{1}{2}}$.

It is further assumed that the data can be described by a function $y = f(x,\underline{a})$, where $\underline{a} = (a_1, a_2, \ldots, a_k)$ is a parameter vector, and it is wished to determine such values of the parameters that the sum of the squares of the differences between the measured y_i values and the function is as small as possible. In other words, the function to minimize is:

$$Q(\underline{a}) = \sum_{i=1}^{m} w_i^2 (y_i - f(x_i, \underline{a}))^2, \qquad (5.3.2.1)$$

and it is assumed that the function Q has a minimum $Q_{min}(\underline{a}) = Q(\underline{a}^*)$. From a starting point $\underline{a}^o$ in the parameter space, a succession of vectors $\underline{a}^n$, n = 1, 2, ... that converges towards the point of minimum $\underline{a}^*$ is sought.

One way of achieving this is to use the method of steepest descent, which consists of choosing the direction of the negative gradient from the point $\underline{a}^p$ and obtaining $\underline{a}^{p+1} = \underline{a}^p - \underline{g}^p$, where

$$g_j^p = \frac{\partial Q(\underline{a}^p)}{\partial a_j} = -2 \sum_{i=1}^{m} w_i^2 (y_i - f(x_i, \underline{a}^p)) \frac{\partial f(x_i, \underline{a}^p)}{\partial a_j} \quad (5.3.2.2)$$

This method is almost certain to yield convergence, but as the search approaches the minimum, the speed of convergence is drastically reduced because of the linear approximation.

An alternative is to use the so-called Newton method. According to this a direction $\underline{h}^p$ in the point $\underline{a}^p$ will be chosen, defined by

$$\underline{\underline{G}}^p \underline{h}^p = - \underline{g}^p \ , \quad (5.3.2.3)$$

obtaining $\underline{a}^{p+1} = \underline{a}^p + \underline{h}^p$. $\underline{\underline{G}}^p$ is a symmetrical matrix that is positive definite when $\underline{a}^p$ is not too far from $\underline{a}^*$. The matrix coefficients are calculated as

$$G_{ij}^p = \frac{\partial^2 Q(\underline{a}^p)}{\partial a_i \partial a_j} = 2 \sum_{i=1}^{m} w_i^2 \left[\frac{\partial f(x_i, \underline{a}^p)}{\partial a_i} \frac{\partial f(x_i, \underline{a}^p)}{\partial a_j} - (y_i - f(x_i, \underline{a}^p) \right.$$

$$\left. \frac{\partial^2 f(x_i, \underline{a}^p)}{\partial a_i \partial a_j} \right] . \quad (5.3.2.4)$$

This method is excellent when $\underline{a}^p$ is close to the solution $\underline{a}^*$, and it has the advantage of yielding quadratic convergence.

The method chosen here consists of a combination of the two aforementioned methods. When the starting point $\underline{a}^o$ is far from $\underline{a}^*$, the minimum is approached by the method of steepest descent, whereafter a modified Newton method is applied.

The Newton method suffers from the disadvantage of the computation of the second derivatives. It is noted, however, that equation (5.3.2.4) consists of a sum of first and second derivatives of $f(x,\underline{a})$. By omitting the second term with the second derivatives in $f(x,\underline{a})$, the computation of the matrix term is considerably simplified. The approximation consists of linearization of $f(x,\underline{a})$ in the point $\underline{a}^p$, which is reasonable when the function slowly varies in the vicinity. This happens to be the case close to the point of minimum $\underline{a}^*$, where the Newton method is most advantageous, so if a point $\underline{a}^p$ is reached where the Newton method would be preferable, choice instead of the

modified Newton method is justified.

The new point $\underline{a}^{p+1}$ is determined by

$$\underline{a}^{p+1} = \underline{a}^{p} + h^{p},$$

where $\underline{h}^{p}$ is calculated from the normal equations:

$$\underline{G}'^{p}\ \underline{h}^{p} = -\underline{g}^{p}, \qquad (5.3.2.5)$$

with

$$G'^{p}_{jr} = \begin{cases} \sum_{i=1}^{m} w_i^2 \dfrac{\partial f(x_i,\underline{a}^{p})}{\partial a_j} \dfrac{\partial f(x_i,\underline{a}^{p})}{\partial a_r} & \text{when } j \neq r \\ \sum_{i=1}^{m} w_i^2 \left(\dfrac{\partial f(x_i,\underline{a}^{p})}{\partial a_j}\right)^2 (1+\lambda) & \text{when } j=r \end{cases} \qquad (5.3.2.6)$$

and

$$-g_j^{p} = \sum_{i=1}^{m} w_i^2 \left(y_i - f(x_i,\underline{a}^{p})\right) \frac{\partial f(x_i,\underline{a}^{p})}{\partial a_j}. \qquad (5.3.2.7)$$

It is noted that $\underline{h}^{p}$ for small positive values of λ ($o < \lambda << 1$) will be found by the modified Newton method, while for great values of λ ($\lambda >> 1$) the diagonal terms in $\underline{G}'^{p}$ will dominate and yield for the j^{th} component of $\underline{h}^{p}$:

$$\lambda \left(\sum_{i=1}^{m} w_i^2 \left(\frac{\partial f(x_i,\underline{a}^{p})}{\partial a_j}\right)^2\right) h_j^{p} = -g_j^{p}, \qquad (5.3.2.8)$$

which directs $\underline{h}^{p}$ towards $-\underline{g}^{p}$ with a value scaled by the diagonal terms and reduced by a factor of λ[30].

At the start of the iterations, a value of λ is chosen that is augmented in the case of increasing values of Q, and thus in turn it results in parameter increments calculated approximately by the method of steepest descent. When the values of Q decrease, λ is gradually reduced, and the parameter increments will tend to be computed according to the modified Newton method Each parameter increment will actually represent an interpolation between the two extremes.

In the present case the function y is expressed by

$$y = B + \sum_{i=1}^{r} P_i \ , \qquad (5.3.2.9)$$

where B represents the background and P_i the i^{th} peak in the fitting interval. It is chosen to represent B by a first-degree polynomial $B = a_1 + a_2x$ because of the poor counting statistics mentioned earlier; a second-degree polynomial would be too sensitive to statistical fluctuations. Each peak is represented by a simple Gaussian function

$$P_i = a_{3+t} \exp\left(-\frac{(x-a_{4+t})^2}{2a_{5+t}^2}\right), \quad \text{where } t = 3\ (i-1). \qquad (5.3.2.10)$$

At high count rates simple Gaussian functions are poor approximations to the peaks, because these will display low-energy "tails" due to pile-up in the detector. Measurements of the environmental gamma radiation, however, are characterized by low count rates.

The fitting function is

$$f(x,\underline{a}) = a_1+a_2x + \sum_{i=1}^{r} a_{3+t} \exp\left(-\frac{(x-a_{4+t})^2}{2a_{5+t}^2}\right) \text{ where } t = 3(i-1), \qquad (5.3.2.11)$$

and with the initial estimates of the $k = 2+3r$ parameters the matrix coefficients and vector coefficients are calculated from equations (5.3.2.6) and (5.3.2.7), and equation (5.3.2.5) is solved to determine the parameter increments, whereafter the process is repeated.

When convergence is achieved the peak parameters are found, and the peak positions are determined by the parameters a_{4+t} while the areas are determined by

$$A_i = a_{3+t} \int_{-\infty}^{\infty} \exp\left(-\frac{(x-a_{4+t})^2}{2a_{5+t}^2}\right) dx = \sqrt{2\pi}\ a_{3+t} \cdot a_{5+t} \ . \qquad (5.3.2.12)$$

The data approximated by the fitting function are the smoothed data and not the original data. The reason for this is that the Poisson distribution of the original data causes the area under the total fit to be consistently underestimated by an amount approximately equal to Q[30]. By smoothing the data Q is considerably reduced, and hereby also the underestimation, and this makes the area determination more accurate.

5.3.3. Error Analysis

The quantity Q is a measure of the goodness of the fit. If the fitting function corresponds exactly to the data, Q will be zero.

In the case of linear least squares fitting, Q is chi-square-distributed and the uncertainties of the parameters are determined from Q and from the diagonal terms of the so-called error matrix, which is obtained by inverting the matrix from the normal equations.

For the non-linear case, there is no exact analytical solution for the determination of the parameter uncertainties, but it is the usual practice to assume the same for the non-linear case as for the linear[27,30-34].

It is thus assumed for the non-linear case that Q is approximately chi-square-distributed with m-k degrees of freedom, and because the expectation value for a chi-square-distributed quantity equals the number of degrees of freedom, there is reason to expect the value of $\frac{Q}{m-k}$ to be close to 1. If $\frac{Q}{m-k} > 1$, the variance of the parameter a_i is estimated to be $\sigma_i^2 = \frac{Q}{m-k} e_{ii}$, where e_{ii} is the i'th diagonal term from the error matrix $\underline{E} = [\underline{G}'^{p}]^{-1}$, and $\underline{G}'^{p}$ the matrix from equation (5.3.2.5) after the last iteration. If $\frac{Q}{m-k} < 1$, the fit is better than statistics would predict, and the variance is estimated to be $\sigma_i^2 = e_{ii}$.

The area A is computed as

$$A = \sqrt{2\pi}\, h \cdot s \,, \qquad (5.3.3.1)$$

where h is the height and s the standard deviation of the Gaussian function. The variance of the area is given by

$$\sigma_A^2 = \left(\frac{\partial A}{\partial h}\right)^2 \sigma_h^2 + \left(\frac{\partial A}{\partial s}\right)^2 \sigma_s^2 \,, \qquad (5.3.3.2)$$

and the uncertainty of the area is calculated from

$$\frac{\sigma_A}{A} = \left\{ \frac{\sigma_h^2}{h^2} + \frac{\sigma_s^2}{s^2} \right\}^{1/2} . \qquad (5.3.3.3)$$

5.3.4. Description of Peak Fitting Procedure

A flow chart for the peak fitting is shown in fig. 5.3.4.1. For each identified peak in the spectrum, a corresponding fitting interval is determined. The width of the interval is chosen to 4 fwhm at the actual energy, i.e., 2 fwhm at each side of the peak. If the distance between two peak positions is less than 2.5 fwhm, both peaks are included in the interval, which is correspondingly increased. No upper limit has been set for the number of peaks in a fitting interval as experience has shown that it is within the capacity of the program to treat the multiplets that appear in spectra from field measurements.

After determining the number of peaks in the fitting interval and the width of the interval, the initial estimates of the parameters are made. If, for example, there are two peaks in the interval, 8 parameters must be estimated - equation (5.3.2.11). The linear background, parameter a_1 and a_2, is determined as the straight line connecting the first and the last data point in the interval. The parameters a_3 and a_6, representing the heights of the Gaussian functions, are taken as the distances from the background to the top of the peaks. The peak positions, parameter a_4 and a_7, have already been determined in the peak search, and finally a_5 and a_8, representing the standard deviations in the Gaussians, are calculated by linear interpolation between input fwhm-values.

These initial parameter estimates form the basis for the first approximation of the data and an example is shown in fig. 5.3.4.2.

In order to solve the normal equations (5.3.2.5), the matrix coefficients and vector coefficients are calculated according to (5.3.2.6) and (5.3.2.7), and furthermore Q is calculated from equation (5.3.2.1). At this point Q is compared to the value from the previous iteration, and if the numerical relative change is less than 0.1%, the iterations are stopped, and the calculation of the uncertainties of the parameters is

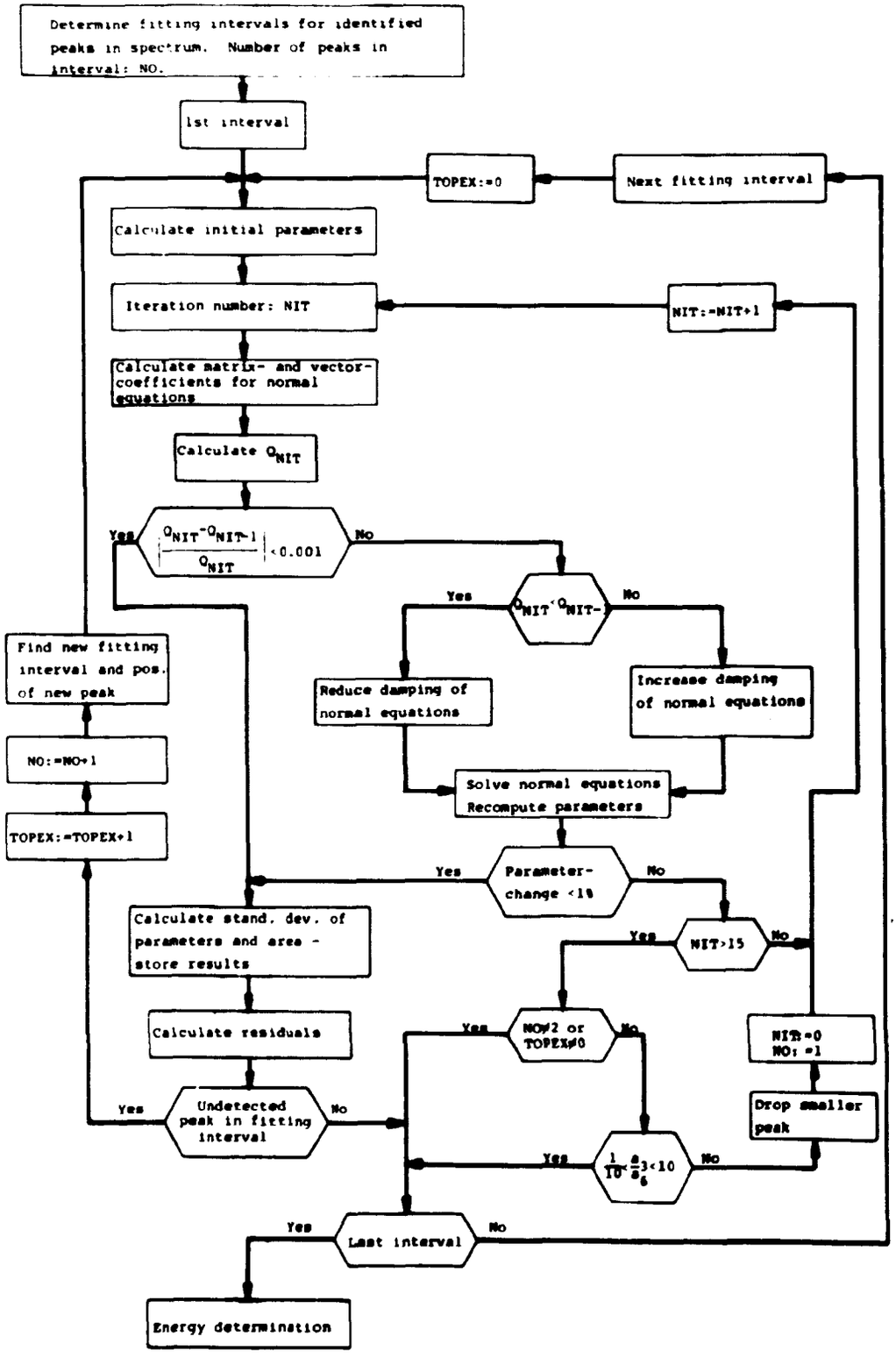

Fig. 5.3.4.1. Flow chart for peak fitting.

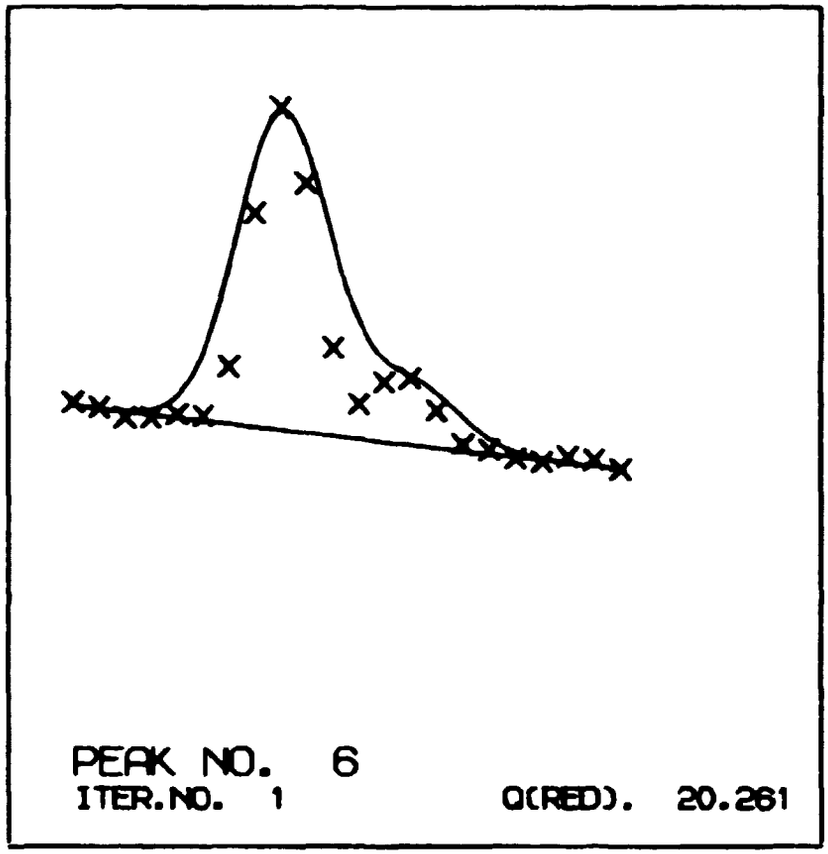

Fig. 5.3.4.2. Initial parameter estimates.

initiated. In the case of the first iteration, Q is compared to zero.

Before the normal equations are solved, they are modified according to the method previously mentioned by multiplying the diagonal terms in the matrix by $1+\lambda$. The initial value of λ is 0.0001 and for each iteration λ is either multiplied by 10 if Q increases, or divided by 10 if Q decreases.

The normal equations are solved and the parameter values recalculated. If the relative change in the parameter values for all the parameters is less than 1%, the iterations are stopped and the uncertainties are computed. If the relative change in any of the parameter values is greater than 1%, a new iteration is started. A maximum of 15 iterations is allowed (with a single exception which will be mentioned later), but usually 5-7 iterations suffice to achieve convergence. The

resulting final parameter estimates from the fit in fig. 5.3.4.2 are shown in fig. 5.3.4.3.

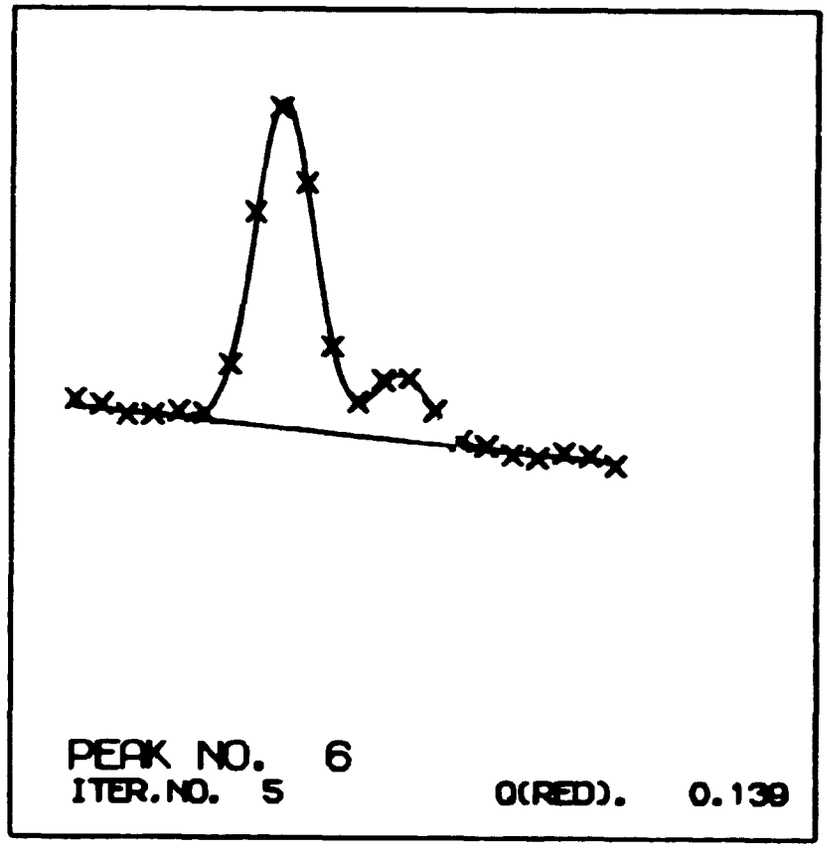

Fig. 5.3.4.3. Final parameter estimates.

The computation of the uncertainties of the results is performed, as explained in section 5.3.3, after the error matrix has been calculated.

The following results are stored: peak position and error, fwhm and error, peak area and error, number of iterations, width of interval m, Q and $\frac{Q}{m-k}$.

A line-printer plot is made of the final result in order to check visually that the fit is satisfactory, fig. 5.3.4.4. For each channel in the fitting interval a plot is made of the background indicated by "B", the content of the channel indicated by "S", the resulting Gaussian function indicated by "G", and the residual indicated by "R", calculated in units of the standard deviation of the channel content. In addition the number of iterations and the value of $\frac{Q}{m-k}$ (QRED) are printed.

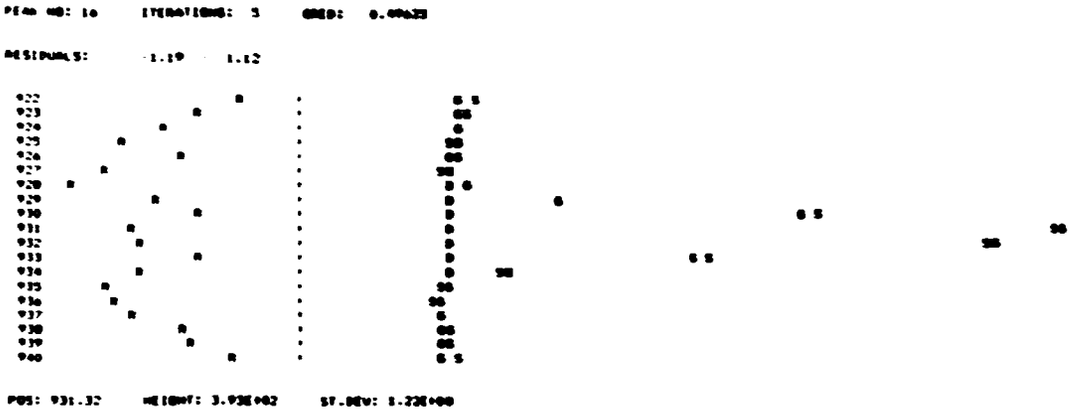

Fig. 5.3.4.4. Lineprinter plot of fit.

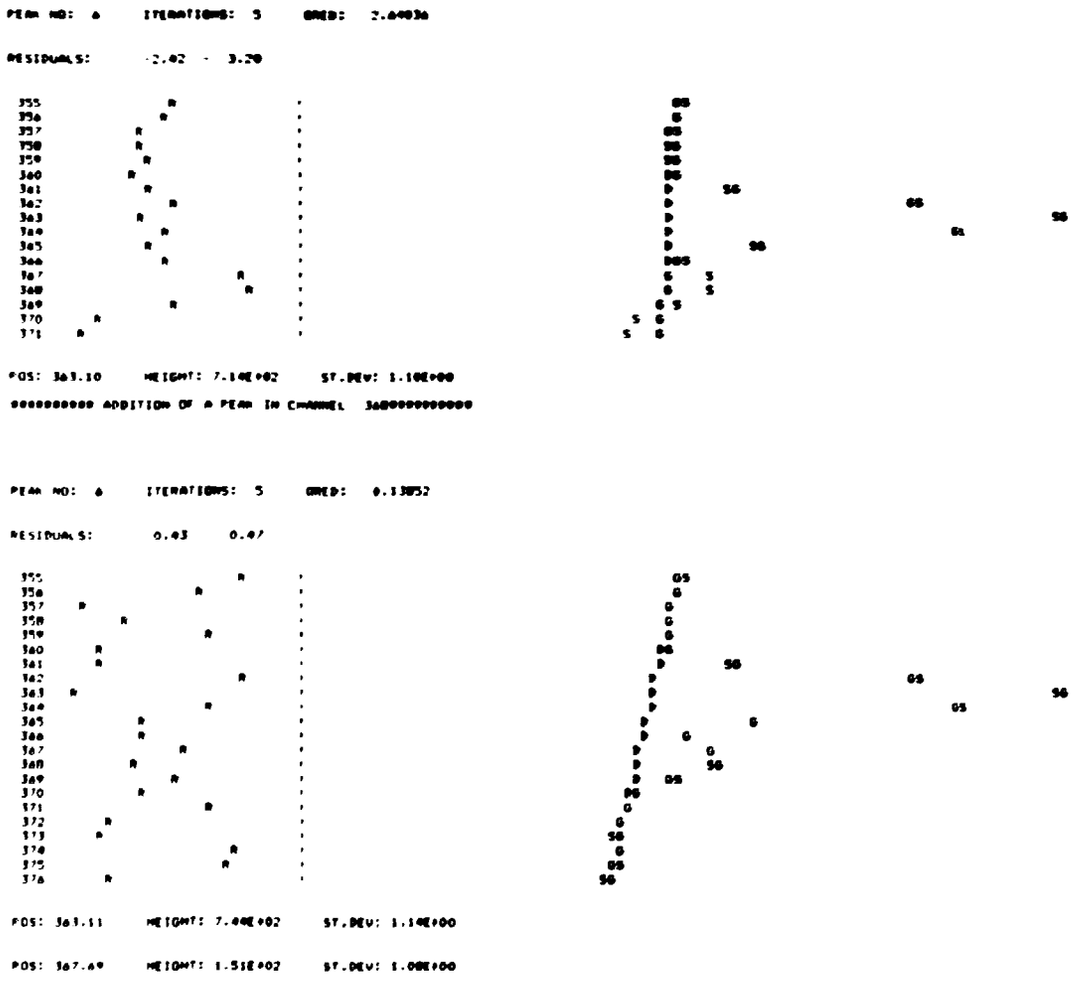

Fig. 5.3.4.5. Lineprinter plot of fit. Addition of undetected peak.

A good fit will be characterized by low values of $\frac{Q}{m-k}(<1)$ and a random variation of the residuals across the fitting interval. In the case of multiplets, it might happen that a peak in the interval remains unidentified and therefore results in $\frac{Q}{m-k}>1$ and a characteristic variation in the residuals - see fig. 5.3.4.5. The residuals are therefore checked for this characteristic variation, and if it is recognized that an extra peak should be added, accounts are kept of the changed number of peaks in the fitting interval and the iterations are re-started with the new peak added. In this way it is possible to analyze multiplets with close-lying peaks - see fig. 5.3.4.6.

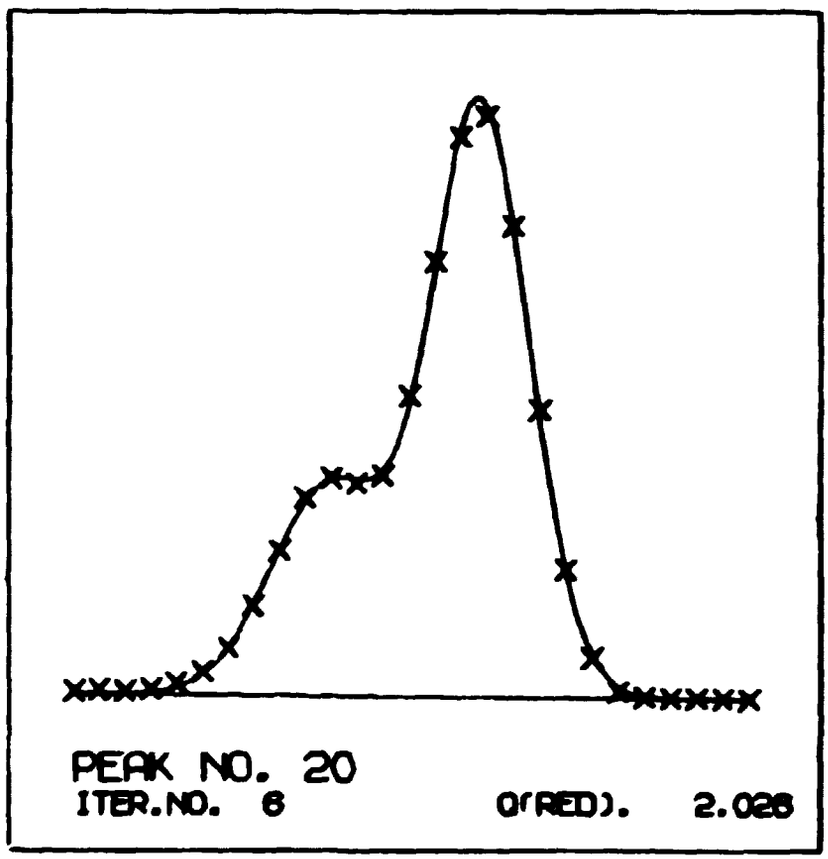

Fig. 5.3.4.6. Plot of doublet with close-lying peaks.

Experience has shown that in the case of fitting-intervals with two peaks convergence problems are often caused by one of the peaks being considerably smaller than the other. Because of poor counting statistics, the parameters for the small peak cannot be determined with the accuracy required for convergence. An attempt is therefore made to obtain a satisfactory fit by

fitting only the larger peak with a Gaussian function, while the small peak is considered as a variation in the background. In this case the residuals are not checked for addition of another peak in the interval.

It sometimes appears that the matrix from the normal equations is not positive definite, and consequently the equations cannot be solved. One more attempt is then made by changing λ to 100 and restarting the computations.

5.4. Energy Determination and Isotope Identification

A flow chart of the remaining computer analysis is shown in fig. 5.4.1.

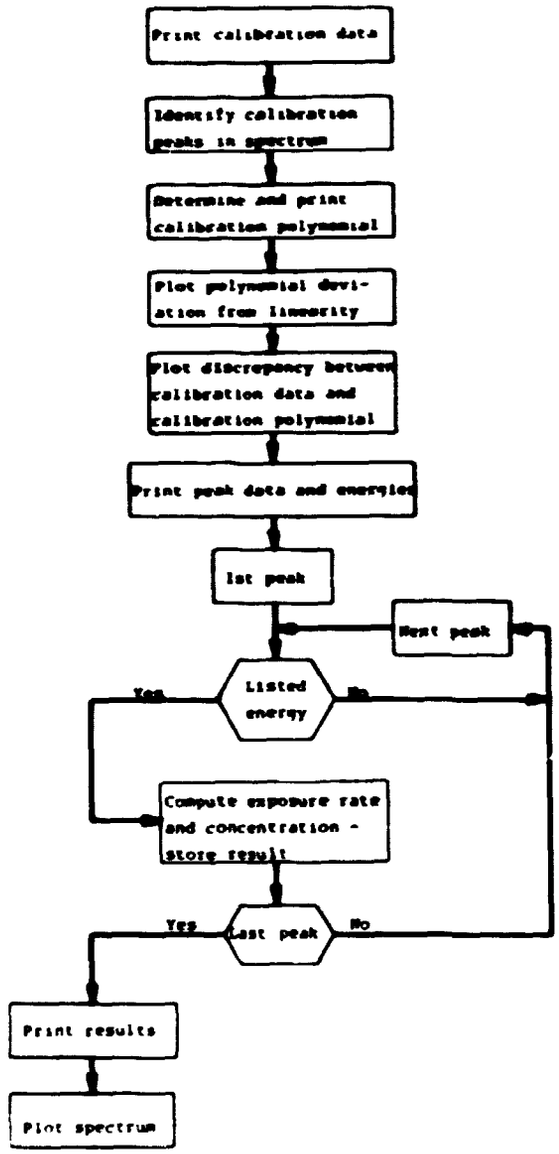

Fig. 5.4.1. Flow chart for energy determination and isotope identification.

After each field measurement the approximate positions of about 20 of the most prominent peaks in the spectrum are noted; all the peaks originate from the naturally occurring radionuclides. These positions and the corresponding energies provide input for a least squares fit with a third-degree polynomial, which establishes the relationship between channel number C and gamma energy E,

$$E = a_o + a_1 C + a_2 C^2 + a_3 C^3 \ . \qquad (5.4.1)$$

In the computations, each set of data is weighted with the reciprocal of the variance of the peak position as calculated from the non-linear least squares fit.

An assessment of the calibration is made on the basis of two line-printer plots. In order to control that the deviation from linearity of the calibration is small, this difference is plotted versus channel number; an example is shown in fig. 5.4.2. The deviation of the calibration from the input data is plotted for each of the calibration peaks; fig. 5.4.3 shows an example.

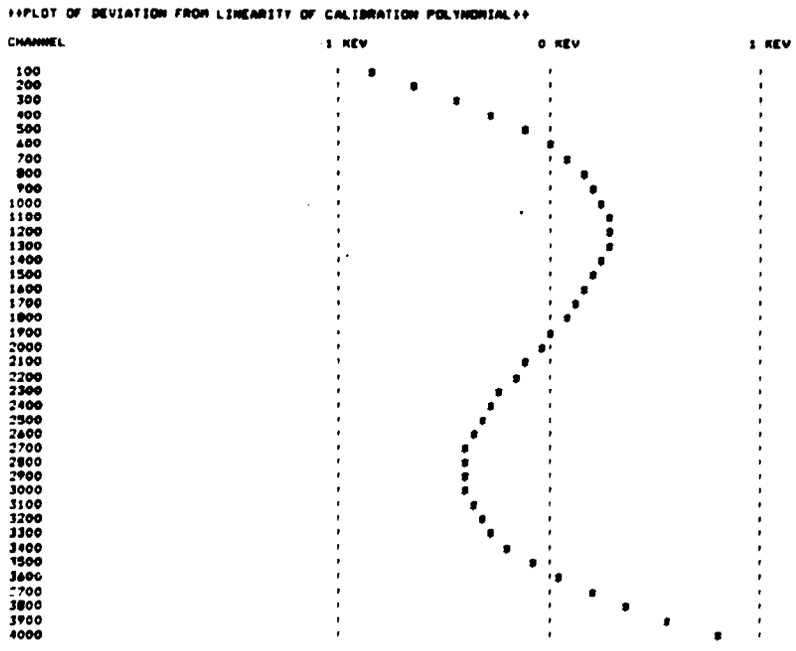

Fig. 5.4.2. Lineprinter plot of deviation of calibration polynomial from linearity.

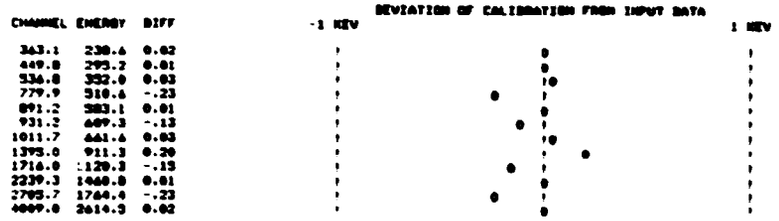

Fig. 5.4.3. Lineprinter plot of deviation of calibration from input data.

For each detected peak in the spectrum, the corresponding gamma energy is compared tc gamma energies from a library representing the naturally occurring radionuclides and a number of fallout radionuclides. Identification takes place when the difference between a listed energy and a measured energy is below 1 keV.

The count rate for each peak identified as belonging to the ^{238}U series or the ^{232}Th series is used to estimate the exposure rate and the concentration in the ground under the assumption of secular equilibrium. The results for each series are combined using a weighted average, and the mean value $\bar{x}$ with the standard deviation $\bar{\sigma}$ is calculated according to:

$$\bar{x} = \frac{\Sigma \frac{x_i}{\sigma_i^2}}{\Sigma \frac{1}{\sigma_i^2}} \qquad (5.4.1)$$

and

$$\bar{\sigma}^2 = \frac{1}{\Sigma \frac{1}{\sigma_i^2}} \quad . \qquad (5.4.2)$$

Figure 5.4.4 shows an example of the computer printout.

A plot of the spectrum, where the detected peaks are marked and the identified peaks supplied with gamma energy and isotope designation, is optional. An example is shown in fig. 3.1.

5.5. Performance of Method of Analysis

Participation in an intercomparison of methods for processing Ge(Li) gamma-ray spectra arranged by the International

RESULTS FOR THE U-238 SERIES

ENERGY KEV	EXPOSURE RATE UR/H	ERROR	CONCENTRATION PCI/G	ERROR
186.1	0.91	0.29	0.48	0.15
293.2	0.67	0.03	0.35	0.04
352.0	0.75	0.04	0.40	0.02
609.4	0.69	0.04	0.37	0.02
934.1	0.80	0.32	0.43	0.17
1120.4	0.70	0.09	0.41	0.05
1238.2	1.12	0.27	0.59	0.14
1377.8	0.74	0.20	0.39	0.10
1509.5	0.83	0.34	0.44	0.18
1764.7	0.79	0.07	0.42	0.04
1847.7	0.76	0.30	0.40	0.16
2204.5	0.79	0.17	0.42	0.09
AVERAGE	0.73	0.02	0.39	0.01

RESULTS FOR THE TH 232 SERIES

ENERGY KEV	EXPOSURE RATE UR/H	ERROR	CONCENTRATION PCI/G	ERROR
270.2	2.05	0.61	0.74	0.22
338.5	0.87	0.16	0.31	0.06
463.0	1.46	0.48	0.52	0.17
583.1	0.94	0.07	0.34	0.03
727.2	0.88	0.23	0.32	0.08
794.9	0.73	0.36	0.27	0.13
860.1	1.40	0.40	0.51	0.14
911.1	0.95	0.07	0.34	0.03
964.5	1.02	0.36	0.37	0.13
968.9	1.11	0.12	0.40	0.04
1588.1	0.92	0.21	0.33	0.08
2614.5	0.97	0.06	0.35	0.02
AVERAGE	0.97	0.04	0.35	0.01

RESULT FOR P-40

ENERGY KEV	EXPOSURE RATE UR/H	ERROR	CONCENTRATION PCI/G	ERROR
1460.8	1.74	0.05	10.59	0.26

RESULT OF DETECTED CESIUM UNDER THE ASSUMPTION OF 11 CM MEAN DEPTH
AND OTHER IDENTIFIED ISOTOPES.

ISOTOPE	ENERGY KEV	EXPOSURE RATE UR/H	ERROR	CONCENTRATION PCI/KM^2	ERROR
CS 137	661.6	0.16	0.01	65.49	2.58
NB 95	765.8				
ZR 95	724.0 756.4				

Fig. 5.4.4. Lineprinter listing of results.

Atomic Energy Agency provided the possibility of a detailed investigation of the performance of the computer program ANSP.

The IAEA will issue an evaluation report after receipt of the results from the participants. This report will analyse the validity of the evaluation method of each participant and permit a comparison of different evaluation methods.

The participants who have reported the results of their analyses of the test spectra have already received the correct results from the IAEA, and have thus been able to make a comparison themselves.

5.5.1. Description of Test Spectra

The test spectra all originate from experimentally recorded gamma spectra that have been subject to manipulations in a computer. Four types of test spectra are represented.

1) One spectrum containing 20 single peaks with a good statistical precision serves as a reference.

2) One spectrum with an unknown number of single peaks close to the limit of detection is used for testing the peak detection abilities of the method of analysis.

3) Six spectra all identical except for differences due to counting statistics and each with 22 single peaks are used for testing the calculations of peak areas and positions.

4) One spectrum containing 9 double peaks with various relative intensities and degrees of overlap is used to test the method of analysis for its ability to resolve the double peaks into their single components.

As the spectra are produced by computer techniques used on original experimental spectra, all the positions and intensities of the peaks relative to those of the reference spectrum are known exactly without any experimental error.

5.5.2. Analysis of Test Spectra

The analysis of the test spectrum for peak detection yielded the result that no spurious peaks were found, while four true peaks were undetected. These peaks were among the smallest and hardly visible on the plot of the spectrum.

The results of the analyses of the six spectra of type three, relative to the results of the analysis of the reference spec-

trum, provided the basis for a detailed statistical analysis of the performance of the peak-fitting method. In each spectrum half of the peaks are situated on a high background and half on a low background, and for each of the two background categories six of the peaks are considerably greater than the remaining five. It was therefore natural to test the peak area evaluation method for the influence of peak size and the influence of level of background, and for possible interactions between the two factors. The 22 peaks in each spectrum were thus divided into 4 groups totalling 24 groups for the six spectra.

In the six spectra one of the peaks on the high background was situated close to the transition between the high and the low background, and the results for this peak had a greater deviation from the corresponding true values than the results for the other peaks. This is explained from the use of a linear background in the peak fitting - see equation (5.3.2.11). As similar background variations do not appear in gamma spectra from field measurements, it was decided to exclude the results for this particular peak from the statistical analysis.

The quantity to be investigated was the ratio of the measured results to the true values. A three-sided analysis of variance of this quantity was performed with the computer program STATDATA[22] testing the variations between the peak sizes, between the levels of the background and between the spectra. No statistically significant variations were observed; in all cases the probability fractile was less than 90%. This indicates that different peak sizes and levels of background do not bias the estimates of the peak areas when calculated by the peak-fitting method.

The ratios of the measured results to the true results for the 126 peaks yielded a mean value of 0.990 ± 0.005 (1 S.E.), which indicates the correctness of the estimated peak areas as the difference from unity is not statistically significant ($P < 95\%$).

The calculated errors of the peak areas and positions were investigated to see how they described the deviations of the measured values from the true values. From statistical theory it is known that if we repeatedly take samples from a normally distributed population and construct 95% confidence intervals for each sample, we can expect 95% of these intervals to contain

the true mean. The width of the 95% confidence interval equals about four standard deviations of the normal distribution, and for the 68% confidence interval it equals about two standard deviations. By considering the computed errors as standard deviations in the above-mentioned sense, confidence intervals were constructed to the measured values of the peak areas and positions, and the number of cases was registered where the intervals included the true values, although these do not necessarily exactly represent the true means. The result is shown in table 5.5.2.1.

Table 5.5.2.1

Comparison between calculated errors of peak data and standard deviations

Interval	Normal distribution	Errors of peak areas	Errors of peak positions
$\pm$ 1 σ	68%	94%	87%
$\pm$ 2 σ	95%	100%	96%

It is seen that the calculated errors of the peak areas and positions are considerably greater than the true standard deviations of the results, and the figures indicate that the calculated errors of the peak areas approximately equal 2 true standard deviations, while for the peak positions the calculated errors approximately equal 1.5 true standard deviations. The reason for the deviation of the calculated errors from the true standard deviations is the non-analytical way of performing the data-fitting, as mentioned in section 5.3.3.

The results of the analysis of the test spectrum with the double peaks showed that the peak-resolving capabilities of the evaluation method were unsatisfactory. Only two of the double peaks were resolved and these were the peaks in the spectrum that displayed the most obvious separation between the single components. The values of the estimated peak areas and positions deviated from the true values more than the calculated errors could account for. An explanation of this poor performance is possibly that a pure Gaussian representation of the data is inadequate for describing peaks with high counting statistics, especially in the case of doublets. Consequently the results of the analyses of multiplets in gamma spectra from field measurements are used with reduced weight.

6. RESULTS

A measuring programme was prepared for the purpose of testing the overall performance of the mobile Ge(Li)spectrometer system. The validity of the results was investigated in two series of measurements: the study of a single location and the country-wide study of 10 locations.

The Risø Health Physics Department annually collects soil samples from all over the country, and the results from the measurements of these samples were compared to the results from the field measurements.

6.1. Comparison of Results of Measurements with NaI(Tl) and Ge(Li) Detectors

Spectroscopic measurements were made with the Ge(Li) detector and the NaI(Tl) detector at 21 locations yielding estimates of the radionuclide concentrations in the ground. Comparison of these results revealed that the values from the NaI(Tl) measurements were considerably higher than those from the Ge(li) measurements. For potassium, uranium and thorium, the ratios between the results from the two types of measurements were 1.07 ± 0.01, 1.40 ± 0.04 and 1.32 ± 0.03, respectively, where the uncertainties equal one standard error of the means.

These discrepancies were not explained by systematic errors in the calibration procedures, and therefore the radionuclide concentrations of the calibration pads shown in table 4.2.1.1 were assumed to be the sources of disagreement. This could be further investigated as Ge(Li) spectroscopic measurements had been made of the calibration pads on the day that the NaI(Tl) detector was calibrated. By relating the measurements of the uncollided gamma flux to the concentrations of the radionuclides in the pads, estimates of these concentrations were obtained based on the calibration of the Ge(Li) detector system.

The measurements were made with the center of the Ge(Li) detector placed 4 cm above the surface of the calibration pads. The spectra were first interpreted as if they had originated from usual field measurements. Corrections were then applied for each full energy peak in the four spectra taking into account the finite size of the calibration pads, the height of

the detector above the pads and the difference in composition between soil and concrete. The corrections were similar to those mentioned in section 4.2.2, but in this case they were exact. The results for the peaks in the two decay series were finally combined for each spectrum using equation (5.4.1). The estimates of the concentrations of the radionuclides are shown in table 6.1.1.

Table 6.1.1

Estimates of the radionuclide concentrations of the calibration pads based on Ge(Li) detector measurements

Pad	% K	ppm U	ppm Th
0	0.75	0.79	1.8
1	6.5	3.1	2.0
2	0.97	6.3	127
3	0.83	156	2.3

Of main importance are the estimates of potassium in pad 1, of uranium in pad 3 and of thorium in pad 2, as they yield the dominating diagonal elements in the matrix $\underline{\underline{C}}$ used for the calculation of the calibration matrix $\underline{\underline{A}}$ in equation (3.2.4). It is seen that these estimates, mentioned in the same order as above, constitute 93%, 87% and 84%, respectively, of the corresponding concentrations listed in table 4.2.1.1 on which the NaI(Tl) detector calibration is based.

At this point it was recognized that the data from table 4.2.1.1 referred to dry weight concentrations and that the potassium concentration of pad 1 was possibly 10% greater than previously reported[35]. This information supported the estimates of concentrations based on the Ge(Li) measurements and indicated a moisture content in the calibration pads of about 15%. On this basis, the results of the NaI(Tl) spectroscopic measurements could not be used for checking the results of the Ge(Li) measurements.

A re-calibration of the NaI(Tl) detector system was performed using the new estimates of the concentrations in the pads. This yielded for the calibration matrix:

$$\underline{\underline{A}}' = \begin{Bmatrix} 3.43 & 0.45 & 0.16 \\ 0.00 & 0.36 & 0.12 \\ 0.00 & 0.01 & 0.14 \end{Bmatrix} . \qquad (6.1.1)$$

The values of the matrix coefficients A_{21}, A_{31} and A_{32} are here in close agreement with the discussion of them given in section 3.2.

The spectroscopic measurements made with the NaI(Tl) detector were re-evaluated using the new calibration, and these results were in better accordance with the Ge(Li) results than previously, but the NaI(Tl) results were still significantly greater than the Ge(Li) results. The average ratios between the results of the two types of measurements were 1.03 ± 0.01, 1.13 ± 0.03 and 1.08 ± 0.02 for potassium, uranium and thorium, respectively, where the uncertainties are standard errors of the means.

These disagreements will be subject to further investigations.

6.2. Investigation of the State of Equilibrium of the ^{238}U Series in Danish Soils

A large number of soil samples from the State experimental farms were subject to investigations of their content of ^{226}Ra and ^{238}U in order to acquire a knowledge of the state of equilibrium of the ^{238}U series in Danish soils. The field spectroscopic measurements will then in turn provide approximate estimates of the ^{238}U concentrations in the soil.

The determinations of the content of ^{226}Ra in the soil samples were made from Ge(Li) spectroscopic measurements in the laboratory. The samples were contained in tin canisters, and secular equilibrium between ^{226}Ra and the principal gamma emitters ^{214}Pb and ^{214}Bi was achieved by ensuring that a minimum of three weeks had elapsed from the closure of the canisters until they were measured. The total error of an individual ^{226}Ra determination consists of a systematic error that is estimated to be 5% plus an error due to counting statistics which typically amounts to 2-3%.

The determinations of the ^{238}U concentrations in the soil were accomplished by irradiation of small samples with thermal neutrons in the research reactor DR 3 at Risø followed by measurements of the delayed neutrons from the fissioning of the ^{235}U nuclei[36]. This technique is based upon the fact that, for natural uranium, the ratio of the concentrations of the two isotopes ^{235}U and ^{238}U is constant. The total error for this determination is estimated to 10%, while the error due to counting statistics alone amounts to 3-4%.

The analyses of 207 soil samples yielded an estimate of the mean value of the ratio between the concentrations of ^{226}Ra and ^{238}U in Danish soils of 0.96 $\pm$ 0.02. The stated standard error of the mean, which is small due to the large number of soil samples, is dominated by the systematic error estimated to 9%. The ^{238}U concentrations in Danish soils (pCi/g) are therefore on the average approximately equal to the corresponding ^{226}Ra concentrations.

6.3. Study of a Single Location

A series of field measurements was performed at Skydebanen, which is a pasture area of approximately 0.1 km^2 that has been used to graze cattle for more than 30 years. The area was chosen because it is situated close to Risø and because it enters into the annual soil sampling programme for the determination of fallout caesium and strontium. Furthermore, as the location has been left undisturbed since the years with high levels of atmospheric fallout, the depth distribution of ^{137}Cs in the soil is well approximated with an exponential distribution, as documented by the laboratory measurements of the soil samples. The ground roughness is characterized as that of an ordinary plowed field, in terms of the categories from table 3.1.5.1, and the particular sites for the field measurements were chosen where larger surface irregularities were minimal. The soil was investigated for its attenuating properties for gamma radiation and the results are given in section 4.1.4.

The purpose of the measurements was to check the reproducibility of the detector system and to investigate the validity of the estimated radionuclide concentrations in the soil.

6.3.1. Results of Field Measurements

A total of six field measurements was performed at Skydebanen and the results are given in table 6.3.1.1.

The evaluation of ^{137}Cs in the soil is based upon the true depth distribution as inferred from the laboratory analyses of soil samples and upon the effects of the ground roughness at the sites.

The exponential distribution of ^{137}Cs in the soil was determined from two depth profiles having a mean relaxation length

Table 6.3.1.1

Results of field measurements at Skydebanen

Date	Counting time (hours)	^{40}K (pCi/g)	^{226}Ra (pCi/g)	^{232}Th (pCi/g)	^{137}Cs (mCi/km^2)
Oct. 7 1976	1.1	10.5±0.3	0.38±0.02	0.44±0.02	69±8
Apr. 15 1977	0.7	10.5±0.4	0.37±0.03	0.44±0.04	78±9
Apr. 15 1977	1.5	10.3±0.7	0.37±0.01	0.47±0.02	73±9
Apr. 19 1977	2.3	10.7±0.2	0.38±0.01	0.45±0.01	70±8
Apr. 25 1977	0.8	10.3±0.3	0.37±0.02	0.38±0.02	98±11
May 15 1977	1.5	10.0±0.3	0.37±0.02	0.42±0.01	57±7
Unweighted mean		10.4	0.37	0.43	74
Standard deviation		0.2	0.01	0.03	14
Standard error		0.1	0.002	0.01	6

of 5.6 cm, which combined with the previously determined soil density of 1.78 g/cm^3 yielded a depth distribution parameter of α/ρ_s = 0.10 cm^2/g. From fig. 4.1.3.1 this parameter value yielded the calibration factor N_f/S_A, which gave estimates of mCi ^{137}Cs per km^2. These estimates were finally corrected for the reduction of the uncollided gamma flux due to the ground roughness as estimated from table 3.1.5.1. A reduction factor of 0.75 was adopted for an ordinary plowed field.

The uncertainties of the results of the individual measurements stated in table 6.3.1.1 are error estimates from the computer analyses of the gamma spectra for the naturally occurring radionuclides, while for ^{137}Cs an additional error of 5% is included due to the uncertainty of the depth distribution parameter α/ρ_s. The relative standard error of the mean value of α was 6% and for ρ_s it was 3%, totalling 7% for α/ρ_s. From fig. 4.1.3.1 it follows that this error of α/ρ_s corresponds to an error of 5% of the value of N_f/S_A in question.

The reproducibility of the estimates of the radionuclide concentrations in the soil is well documented from the results of the measurements that cover a period of more than 7 months. The reason for the interval of 6 months between the first and the second measurement is that shortly after the first measurement the detector suffered a malfunction of an electrical connection inside the cryostat. This was especially inconvenient as the analysis of the first gamma spectrum from Skydebanen revealed the presence of shortlived fallout isotopes: ^{131}I,

^{132}I, ^{140}Ba and ^{140}La. The fresh fallout originated from the first passage of the cloud of debris from an atmospheric nuclear weapons test performed by the People's Republic of China on 26 September 1976. The quantitative results of the field measurements of these isotopes were in reasonable agreement with the gamma spectroscopic measurements performed in the laboratory of precipitation collected in the same period. The detector was returned to the manufacturer for repair. This took almost four months and resulted in a replacement of the detector crystal.

6.3.2. Results of Laboratory Measurements

Gamma spectroscopic measurements were made in the laboratory of two types of soil samples from Skydebanen with the intention of comparing these results with the results from the field measurements. The two types were untreated soil samples and treated soil samples.

Measurements of untreated soil samples yielded results that are most directly compared with the results of the field measurements as the latter refer to in situ soil. Measurements of treated soil samples were made as part of the regular programme of investigating the accumulated fallout in the soil.

The sampling technique consisted of the collection of 8 cores with a diameter of 62 mm whereafter the individual depth segments were composited. The treated samples were allowed to dry in the laboratory for a few days, whereafter the part that passed a 2 mm mesh was baked at 100°C for 24 hours and finally homogeneized for 4 hours in a blending machine. Thus larger particles, e.g., stones, are not included in the samples.

The measurements of the soil samples were made as outlined in section 6.2. With regard to ^{137}Cs, the total activity in each sample was estimated and related to the total area of the 8 cores and this gave estimates of mCi ^{137}Cs per km^2 at the different depth intervals in the soil. The results of two such profiles of the ^{137}Cs distribution are shown in table 6.3.2.1.

Table 6.3.2.1

^{137}Cs distribution in soil from Skydebanen (mCi/km^2)

	0-10 cm	10-20 cm	20-30 cm	Σ 0-30 cm	Relaxation length (cm)
1975	57	14	2	73	6.0
1977	43	9	1	53	5.3

The mean value of the two estimated relaxation lengths was used for evaluating the ^{137}Cs concentrations from the field measurements.

The results of the measurements of the treated soil samples collected at Skydebanen from 1971-1977 are shown in table 6.3.2.2, and the results of the measurements of five untreated soil samples are shown in table 6.3.2.3.

Table 6.3.2.2

Results of laboratory measurements of treated soil samples collected at Skydebanen

	1971	1972	1973	1974	1975	1977	Mean	SD	SE
^{40}K (pCi/g)	16.2	16.1	16.4	15.2	13.1	-	15.4	1.4	0.6
^{226}Ra (pCi/g)	0.53	0.56	0.50	0.55	0.51	-	0.53	0.03	0.01
^{232}Th(pCi/g)	0.62	0.63	0.58	0.69	0.62	-	0.63	0.04	0.02
^{137}Cs(mCi/km^2)	95	77	87	93	75	53	80	16	6

Table 6.3.2.3

Results of laboratory measurements of untreated soil samples collected at Skydebanen in 1977

	1	2	3	4	5	Mean	SD	SE
^{40}K (pCi/g)	10.4	9.7	10.2	12.5	13.1	11.2	1.5	0.7
^{226}Ra (pCi/g)	0.38	0.34	0.37	0.33	0.38	0.36	0.02	0.01
^{232}Th (pCi/g)	0.43	0.40	0.44	0.43	0.49	0.44	0.03	0.01

6.3.3. Comparison of Results

It is difficult to assess how well the collected soil samples represent the soil that is measured in a field measurement. The area contributing to the uncollided gamma flux 1 m above ground is quite large even for uniformly distributed sources, but the depth in the soil from where this flux originates varies considerably with gamma-ray energy and with the distance to the detector. This is depicted in fig. 6.3.1.1, which shows the depths in the soil from where the uncollided gamma flux is attenuated 90% and 50%, respectively, for various gamma-ray energies as a function of the horizontal distance to the detector. For simplicity, the attenuation in air is neglected.

For gamma rays with an energy of 1500 keV entering the detector at an angle of 45°, which means that they originate from the soil 1 m horizontally from the detector, the figure shows

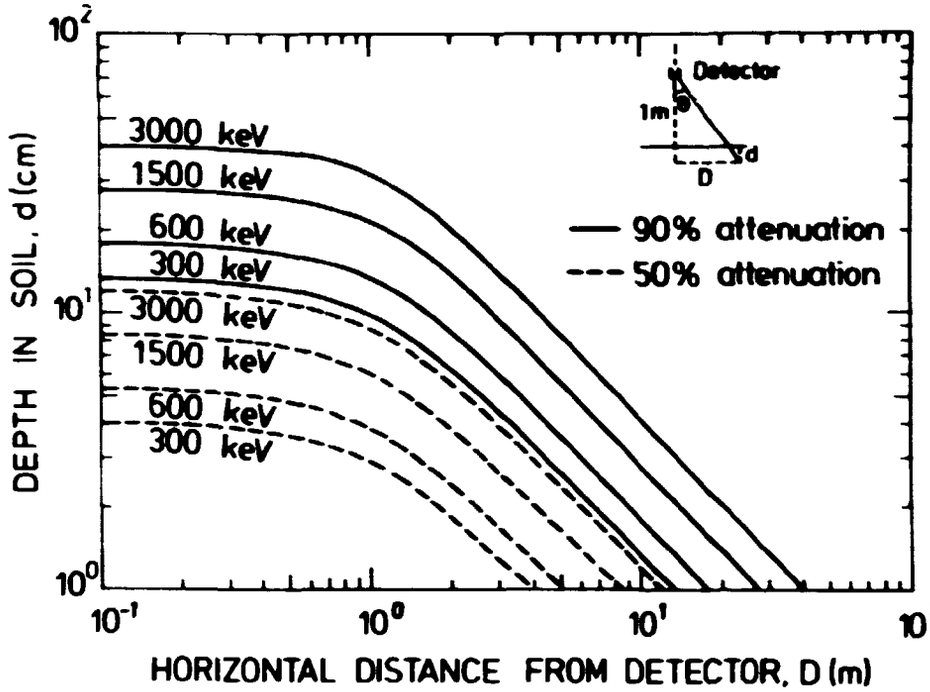

Fig. 6.3.1.1. Depths in soil (cm) where the uncollided gamma flux for various gamma-ray energies is attenuated 90% and 50%, respectively, as a function of horizontal distance to the detector (m).

that more than 90% of this uncollided flux comes from the first 20 cm of the soil and that more than 50% of this flux comes from the first 6 cm. The angular distribution of the uncollided gamma rays causes 2/3 of this flux to originate more than 1 m horizontally from the detector for uniformly distributed sources, and for exponentially and surface-distributed sources this fraction is greater than 2/3. This means for the naturally occurring radionuclides that the first 10 cm of the soil yields a dominating contribution to the uncollided gamma flux 1 m above ground, while for exponentially distributed ^{137}Cs it is the first 2 cm only.

The untreated soil samples were collected from the first 20 cm of the soil and composited as the intention was to compare the results for the naturally occurring radionuclides only.

As seen from tables 6.3.1.1 and 6.3.2.3, the differences between the mean concentrations of ^{40}K, ^{226}Ra and ^{232}Th are not statistically significant, and the comparison therefore yields no basis for not accepting the assumption that the results of the field measurements give the true radionuclide concentrations

for in situ soil, accepting the results of the laboratory measurements as valid.

Comparison of the results for the naturally occurring radionuclides from the field measurements and from the laboratory measurements of the treated soil samples (table 6.3.2.2) shows that the laboratory measurements yield considerably higher results than the field measurements, while for ^{137}Cs the results for the two types of measurement are not significantly different.

It must be emphasized, however, that the values of the ^{137}Cs concentrations from the field measurements depend upon the reduction factor, which describes the gamma flux reduction arising from the ground roughness at the site, and the choice of an appropriate reduction factor relies on a somewhat subjective judgement of the surface conditions at the site.

With respect to the naturally occurring radionuclides, the ratios between the mean values of the results for the field measurements and for the laboratory measurements are 0.68 ± 0.03, 0.70 ± 0.02 and 0.68 ± 0.04 for ^{40}K, ^{226}Ra and ^{232}Th, respectively, where the uncertainties are standard errors. The insignificant differences between the ratios indicate that the results from the field measurements are as self-consistent as the results from the laboratory measurements, but the average ratio of 0.69 represents a considerable difference between the two types of measurement. The difference is probably explained by the fact that the field measurements refer to in situ soil, while the laboratory measurements refer to treated soil.

In order to obtain a quantitative estimate of the fraction that is removed from the soil samples during treatment, 12 samples from Skydebanen were investigated and the ratios of the weights of the samples after treatment to the weights before treatment yielded a mean value of 0.61 ± 0.02 (1 S.E.). This means that on the average 39% of the soil collected was not included in the treated soil samples.

The ratio between the concentrations of naturally occurring radionuclides in the untreated soil and in the soil after treatment depends on the concentrations in the fractions removed. If the concentrations were negligible, the ratio would be expected to approximate a value of 0.61 and if the concentrations were dominant, the ratio would be expected to exceed

unity. Therefore the observed ratio of 0.69 between the results of the field measurements and the results of the laboratory measurements is possibly explained by relatively low concentrations of naturally occurring radionuclides in the discarded stones compared to the concentrations in the remaining soil.

It must be noted that in the case of fallout the results for the two types of measurement are directly comparable, as the part of the collected soil samples that is removed only contains sources of natural origin.

6.4. Country-wide Measurement

A series of field measurements was performed in June 1977 at 10 of the State experimental farms, which are situated as shown in fig. 6.4.1.

The purpose of the measurements was to quantify all detected radionuclides at the sites and to compare these results with the results from the laboratory measurements of the collected soil samples, and furthermore to investigate the validity of the exposure rate estimates as evaluated from the field spectroscopic measurements.

6.4.1. Results of Field Measurements

In 1975 a detailed soil sampling programme was carried out where samples were collected of both cultivated soils and uncultivated soils at the State experimental farms. It was thus intended to perform the field measurements at the sites from where the soil samples were collected in 1975 and accordingly to make two field measurements at each locality.

While carrying out the on-site measuring programme it was discovered that the majority of the previously uncultivatd soils had been cultivated since the samples were collected in 1975. Nevertheless it was decided to make measurements at these locations as the only effect of cultivation is to alter the depth distribution of the fallout radionuclides in the plowing layer.

The results for the naturally occurring radionuclides are shown in table 6.4.1.1.

It is noted that the results for the two sites at each locality are generally in good agreement. This was to be expected as the distance between the two sites only exceeded 1 km in the case of Abed.

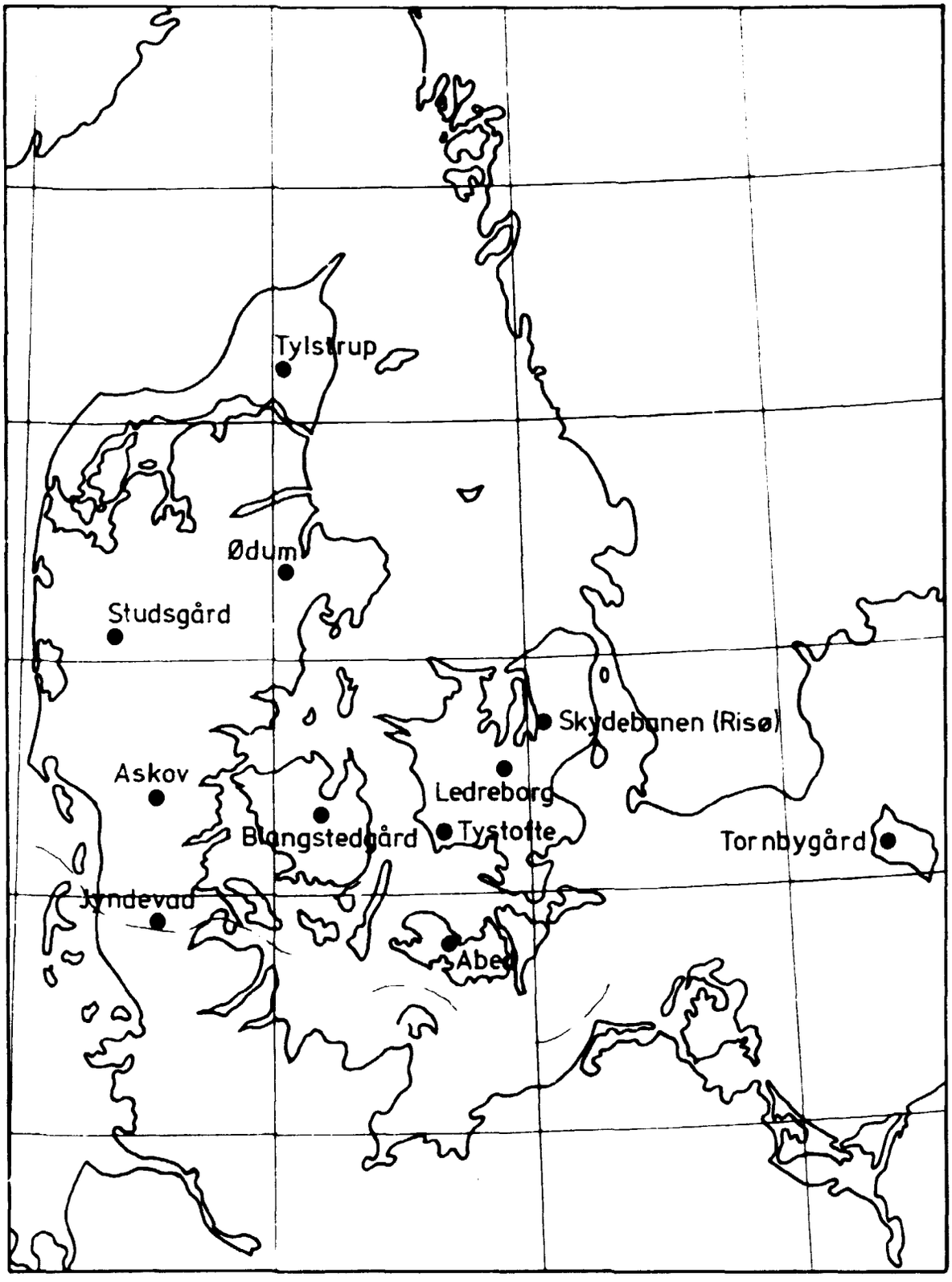

Fig. 6.4.1. State experimental farms in Denmark.

Table 6.4.1.1

Naturally occurring radionuclides in the soil at the State experimental farms and at Skydebanen estimated from field measurements (pCi/g)

	Nuclide	Tylstrup	Studsgård	Ødum	Askov	Jyndevad	Blangstedgård	Tystotte	Ledreborg	Skydebanen	Abed	Tornbygård	Mean	SD	SE
Cultivated	^{40}K	10.4	5.6	13.2	9.7	7.3	12.9	14.2	13.1	-	12.5	14.9	11.4	3.1	1.0
	^{226}Ra	0.36	0.32	0.50	0.36	0.18	0.47	0.55	0.46	-	0.53	0.58	0.43	0.12	0.04
	^{232}Th	0.30	0.20	0.50	0.44	0.18	0.52	0.59	0.54	-	0.57	0.70	0.45	0.17	0.05
Uncultivated	^{40}K	10.6	5.9	10.7	8.4	7.2	10.4	14.0	13.2	10.4	6.5	11.8	9.9	2.7	0.8
	^{226}Ra	0.39	0.19	0.43	0.31	0.18	0.46	0.52	0.71	0.37	0.29	1.37	0.47	0.33	0.10
	^{232}Th	0.35	0.20	0.43	0.35	0.17	0.39	0.58	0.53	0.43	0.34	0.67	0.40	0.15	0.05

On two occasions, however, the field measurements were made during rainfall and this caused a wash-out of the radon daughters in the air. In these cases (Studsgård cultivated soil and Ledreborg uncultivated soil) the soil content of ^{226}Ra was overestimated because of the surface deposition of radon daughters.

The measurement at Tornbygård of uncultivated soil yielded a significantly higher ^{226}Ra concentration than the measurement of cultivated soil. A possible explanation for this is that the site of the uncultivated soil was very close (< 30 m) to a spring whose water is known by local people to contain radium, but no investigation was made of this matter.

The significant difference between the results for the two sites at Abed was caused by the atypical soil composition at the site of the uncultivated soil. It had a large content of organic matter with a correspondingly small content of minerals.

The results for the fallout radionuclides ^{137}Cs, ^{95}Zr and ^{95}Nb are shown in table 6.4.1.2.

For the cases where the measurements were made over arable land, the distribution of ^{137}Cs was known to be uniform down to a depth of 20 cm corresponding to the depth of the plowing layer. Furthermore, as the detector in a field measurement would only register negligible contributions from ^{137}Cs buried deeper than 20 cm (fig. 6.3.1.1), it was justified to consider the distribution of ^{137}Cs as uniform overall, and the concentrations are therefore given in pCi/g.

Only for uncultivated soil at Skydebanen and at Studsgård

Table 6.4.1.2

Fallout radionuclides in the soil at the State experimental farms and at Skydebanen estimated from field measurements

	Nuclide	Unit	Tylstrup	Studsgård	Ødum	Askov	Jyndevad	Blangstedgård	Tystofte	Lerbjerg	Skydebanen	Abed	Tornbygård	Mean	SD	SE
Cultivated	^{137}Cs	pCi/g	0.23	0.25	0.19	0.21	0.24	0.22	0.17	0.14	-	0.15	0.17	0.20	0.04	0.01
	^{95}Zr	mCi km^{-2}	1.6	2.8	2.2	2.2	2.4	2.2	2.8	ND	-	ND	2.0	2.2	0.5	0.2
	^{95}Nb	mCi/km^2	2.2	4.4	3.8	4.2	4.6	3.2	3.8	ND	-	2.8	2.4	3.3	0.9	0.3
Uncultivated	^{137}Cs	pCi/g	0.29		0.46	0.31	0.19	0.56	0.16	0.13		0.26	0.27	0.29	0.14	0.05
	^{137}Cs	mCi/km^2		260*							76*					
	^{95}Zr	mCi km^{-2}	2.8	3.2	2.0	2.8	2.6	2.2	1.2	1.0	1.2	1.2	1.6	2.0	0.8	0.2
	^{95}Nb	mCi/km^2	2.4	6.4	4.0	4.6	5.2	3.6	2.0	2.4	2.4	1.6	3.0	3.4	1.5	0.5

ND: not detected
* Calculated from a depth distribution parameter of α/ρ_s = 0.10 cm^2/g

was the distribution well approximated with an exponential distribution; at both locations with a depth distribution parameter of α/ρ_s = 0.10 cm^2/g. At Studsgård the rather high estimate of 260 mCi/km^2 was probably caused by a thick covering of heather at the site. Like lichen, heather is a perennial plant with a large surface and it might therefore accumulate fallout. The covering of heather would thus represent a source elevated above ground and therefore yield a significant contribution to the 662 keV gamma flux 1 m above ground.

The fallout radionuclides ^{95}Zr and ^{95}Nb originating from the atmospheric nuclear weapons test performed on 17 November 1976 by the People's Republic of China were assumed to be distributed directly on the surface of the ground. The concentrations were close to the limits of detection and the evaluation of the peak areas was furthermore complicated by the presence of close-lying peaks from the naturally occurring radionuclides. As the gamma-ray energies of ^{95}Zr and ^{95}Nb are only about 100 keV higher than the gamma-ray energy of ^{137}Cs, the results were evaluated using the reduction factors from table 3.1.5.1 to account for the ground roughness at the sites. It is noted that the ratios between the concentrations of the two nuclides at the sites reasonably well approximate a value of 1.9, which is the theoretical ratio between the nuclide

concentrations corrected for a period of 7 months elapsing since their formation.

It is believed that the relatively high estimates of ^{95}Zr and ^{95}Nb for the uncultivated soil at Studsgård are caused by the covering of heather, as mentioned above.

The results for the estimates of exposure rates are given in table 6.4.1.3.

Table 6.4.1.3

Estimates of exposure rates at the State experimental farms and at Skydebanen (μR/h)

Locality		^{40}K	^{238}U series	^{232}Th series	Fallout	Terrestrial exposure rate	Total exposure rate	Difference
Tylstrup	cult.	1.9	0.7	0.8	0.1	3.5	7.6	4.1
	uncult.	1.9	0.7	1.0	0.2	3.8	8.0	4.2
Studsgård	cult.	1.0	0.6	0.6	0.2	2.4	6.6	4.2
	uncult.	0.7	0.4	0.6	0.7	2.4	6.9	4.5
Ødum	cult.	2.4	0.9	1.4	0.1	4.8	9.0	4.2
	uncult.	2.0	0.8	1.2	0.3	4.3	8.5	4.2
Askov	cult.	1.8	0.7	1.2	0.1	3.8	8.1	4.3
	uncult.	1.5	0.6	1.0	0.2	3.3	7.5	4.2
Jyndevad	cult.	1.3	0.3	0.5	0.1	2.2	6.6	4.4
	uncult.	1.3	0.3	0.5	0.1	2.2	6.5	4.3
Blangstedgård	cult.	2.4	0.9	1.5	0.1	4.9	8.9	4.0
	uncult.	1.9	0.9	1.1	0.3	4.2	8.5	4.3
Tystofte	cult.	2.6	1.1	1.6	0.1	5.4	9.5*	4.1
	uncult.	2.6	1.0	1.6	0.1	5.3	9.3*	4.0
Ledreborg	cult.	2.4	0.9	1.5	0.1	4.9	9.0*	4.1
	uncult.	2.4	1.3	1.5	0.1	5.3	9.4*	4.1
Skydebanen	uncult.	1.8	0.7	1.2	0.1	3.8	8.2*	4.4
Abed	cult.	2.3	1.0	1.6	0.1	5.0	9.2*	4.2
	uncult.	1.2	0.6	1.0	0.2	3.0	6.9*	3.9
Tornbygård	cult.	2.7	1.1	2.0	0.1	5.9	10.1	4.2
	uncult.	2.2	2.6	1.9	0.2	6.9	10.7	3.8
Mean		1.9	0.9	1.2	0.17	4.2	8.3	4.18
SD		0.6	0.5	0.4	0.14	1.3	1.2	0.17
SE		0.1	0.1	0.1	0.03	0.3	0.3	0.04

* Measured with a high pressure ionization chamber

For each locality, the individual contributions from the naturally occurring radionuclides and from the fallout radionuclides are given as estimated from the recorded gamma spectra. The sum of these contributions yields the terrestrial gamma exposure rate. The total exposure rate at the sites is estimated from measurements made with the NaI(Tl) detector used as a total count scintillometer (described in section 4.3), and in a few cases direct measurements were made with the high pressure ionization chamber. Finally, the difference between the estimates of the total exposure rate and the terrestrial exposure rate is given for each locality.

On the average it is estimated that the terrestrial exposure rate consists of a contribution of 45% from ^{40}K, 22% from the ^{238}U series, 29% from the ^{232}Th series and 4% from fallout.

6.4.2. Results of Laboratory Measurements

The soil samples collected in 1975 at the State experimental farms were taken down to a depth of 50 cm. For the cultivated soils, the samples were taken from 0-20, 20-30 and 30-50 cm and for the uncultivated soils from 0-10, 10-20, 20-30 and 30-50 cm.

The samples were collected and treated as outlined in section 6.3.2.

The mean values of the results from 0-50 cm are given in table 6.4.2.1.

Table 6.4.2.1

Results of laboratory measurements of soil samples collected in 1975 at the State experimental farms and at Skydebanen (pCi/g)

	Nuclide	Tylstrup	Studsgård	Ødum	Askov	Jyndevad	Blangstedgård	Tystofte	Ledreborg	Skydebanen	Aked	Tornbygård	Mean	SD	SE
Cultivated	^{40}K	9.4	6.6	14.7	9.9	10.6	13.7	13.7	16.0	-	13.5	16.6	12.6	3.2	1.0
	^{226}Ra	0.26	0.23	0.45	0.37	0.29	0.59	0.57	0.56	-	0.56	0.79	0.47	0.18	0.06
	^{232}Th	0.25	0.22	0.52	0.37	0.29	0.64	0.65	0.75	-	0.70	0.81	0.52	0.22	0.07
	^{137}Cs*	0.28	0.28	0.24	0.28	0.21	0.20	0.24	0.17	-	0.15	0.19	0.22	0.05	0.01
Uncultivated	^{40}K	11.5	5.9	10.9	8.7	6.5	11.7	13.5	15.6	13.3	11.8	9.3	10.8	3.0	0.9
	^{226}Ra	0.32	0.27	0.34	0.33	0.14	0.84	0.46	0.53	0.52	0.67	1.03	0.50	0.25	0.08
	^{232}Th	0.30	0.29	0.35	0.34	0.15	0.47	0.48	0.65	0.62	0.65	0.58	0.44	0.17	0.05

*Values for 0-20 cm

For comparison with the results of the field measurements, only the values for ^{137}Cs for cultivated soils from the depth 0-20 cm are used, and for the uncultivated soils the values are omitted as the two types of measurement yielded incomparable results.

A sample was collected at Skydebanen of surface soil on 18 May 1977 for the determination in the laboratory of the concentrations of ^{95}Zr and ^{95}Nb. The results yielded estimates of 1.4 mCi/km^2 of ^{95}Zr and 2.8 mCi/km^2 of ^{95}Nb.

6.4.3. Comparison of Results

The results of the two types of measurements were combined by forming the ratios between the results of the field measurements and the results of the laboratory measurements. An analysis of variance of these ratios made by the computer program STATDATA, showed no significant variation between the cultivated soils and the uncultivated soil, and the ratios were therefore composited for each nuclide at each locality. The mean values are shown in table 6.4.3.1, and the result of the analysis of variance of these ratios is shown in table 6.4.3.2, where SSD denotes the sum of squares of deviation: $\Sigma(\bar{x}-x_i)^2$, f the degrees of freedom, s^2 the variance, v^2 the ratio between the variance in question and the residual variance, and P the probability fractile of the distribution in question.

The variation between nuclides was not significant (P < 90%), but the variation between locations was highly significant (P > 99.99%). As seen from table 6.4.2.2, the mean of the ratios varied from 0.73 at Skydebanen to 1.12 at Tystofte.

Table 6.4.3.1

Average values of ratios between results of the field measurements and results of the laboratory measurements of soil from the State experimental farms and from Skydebanen

Nuclide	Tystofte	Studsgård	Ødum	Askov	Jyndevad	Blangstedgård	Tystofte	Ledreborg	Skydebanen	Abed	Tornbygård	Mean
^{40}K	1.03	0.97	0.95	0.97	0.95	0.91	1.04	0.84	0.78	0.71	1.13	0.94
^{226}Ra	1.38	1.00	1.21	0.97	1.10	0.66	1.06	1.12	0.71	0.66	1.12	1.00
^{232}Th	1.26	0.90	1.11	1.10	0.99	0.83	1.08	0.78	0.70	0.66	1.07	0.94
^{137}Cs	0.82	0.89	0.79	0.75	1.14	1.10	0.71	0.82	-	1.00	0.89	0.89
Mean	1.12	0.92	1.02	0.95	1.05	0.88	0.97	0.89	0.73	0.76	1.05	0.94

Table 6.4.3.2

Analysis of variance of the ratios between the results of the field measurements and the results of the laboratory measurements

Variation	SSD	f	s^2	v^2	P
Between nuclides	0.301	3	0.100	1.74	<90%
Between locations	4.557	10	0.456	7.90	>99.99%
Remainder	10.388	180	0.058		

In section 6.3.3 a mean ratio of 0.69 was obtained at Skydebanen by comparing the results of the field measurements with the results of the laboratory measurements averaged over five years. It was pointed out that the low value of the ratio might be explained by the removal of stones during treatment of the collected soil, assuming that the concentrations in the stones of the naturally occurring radionuclides were significantly lower than the concentrations in the remaining soil.

It is believed that the significant variations observed between the locations in this study are due to differences in soil composition of the above mentioned nature, but the matter remains to be further investigated.

The estimated concentrations of ^{95}Zr and ^{95}Nb at Skydebanen evaluated from the field measurement made on 15 May agree well with the results of the laboratory measurements made of the soil samples collected on 18 May. The levels of fresh fallout in the western part of the country seem to be somewhat higher than in the eastern part, which is in agreement with observations of the precipitation.

6.4.4. Overestimates of ^{226}Ra in the Soil due to Radon Daughters in the Air

The atmospheric concentrations of radon daughters will, as previously mentioned, cause the field measurements to yield too high estimates of ^{226}Ra in the soil. A quantitative evaluation of these overestimates is possible from a knowledge of these atmospheric concentrations.

Measurements of outdoor concentrations in Denmark of radon daughters in the air have yielded values of typically 0.01 pCi/l under conditions of normal atmospheric turbulence[37]. In these

cases it is justified to assume constant concentrations in the lower atmosphere[18], and the resulting uncollided gamma fluxes at ground level are therefore calculated from a semi-infinite cloud model.

The uncollided gamma flux, ϕ, at ground level is given by:

$$\phi = \int_0^{\infty} \int_0^{\pi/2} S(4\pi R^2)^{-1} \exp(-\mu_a R) 2\pi R^2 \sin\theta \, d\theta \, dR, \quad (6.4.4.1)$$

where S is the atmospheric concentration of radon daughters, μ_a the linear attenuation coefficient for gamma rays in the air, R the distance from the detector to the infinitesimal volume element, and θ the angle between vertical and the R-vector. The integration yields:

$$\phi = S/(2\mu_a), \quad (6.4.4.2)$$

and by inserting the gamma yield f, ϕ is expressed in units of photons/cm^2/s:

$$\phi = 3.7 \cdot 10^{-5} \cdot f \cdot S/(2\mu_a), \quad (6.4.4.3)$$

where f is in units of photons/disintegration, S in units of pCi/l and μ_a in units of cm^{-1}.

As the gamma rays of 352 keV and 609 keV from ^{214}Pb and ^{214}Bi, respectively, are the most dominant, only the gamma fluxes for these energies are calculated.

352 keV: $S = 0.01$ pCi/l

$f = 0.35$ photons/dis.

$\mu_a = 1.2 \cdot 10^{-4}$ cm^{-1}

$\phi = 5.4 \cdot 10^{-4}$ photons/cm^2/s

609 keV: $S = 0.01$ pCi/l

$f = 0.43$ photons/dis.

$\mu_a = 1.0 \cdot 10^{-4}$ cm^{-1}

$\phi = 8.0 \cdot 10^{-4}$ photons/cm^2/s

The response of the Ge(Li) detector to sources in the upper

half-space is smaller than the response to sources in the lower half-space because of the additional shielding from the detector cryostat and the dewar. The angular correction factors, N'_f/N_o, for the upper half space were determined experimentally with a point source and yielded values of 0.82 and 0.83 for the energies 352 keV and 609 keV, respectively. The resulting full energy peak count rates, N'_f, from concentrations of 0.01 pCi/l of radon daughters are thereby obtained:

$$N'_f = (N'_f/N_o)(N_o/\phi)\phi,$$

$$352 \text{ keV: } 0.82 \cdot 6.20 \cdot 5.4 \cdot 10^{-4} = 2.7 \cdot 10^{-3} \text{ cps}$$

$$609 \text{ keV: } 0.83 \cdot 3.60 \cdot 8.0 \cdot 10^{-4} = 2.4 \cdot 10^{-3} \text{ cps}$$

If these count rates are interpreted in terms of ^{226}Ra in the soil, both energies yield estimates of 0.0073 pCi/g.

It is therefore seen that atmospheric concentrations of 0.01 pCi/l of radon daughters during a field measurement cause the concentrations of ^{226}Ra in the soil to be overestimated by an amount of 0.0073 pCi/g, which compared to the average concentration in Danish soils of 0.45 pCi/g amounts to 1.6%. At Jyndevad atmospheric concentrations of 0.05 pCi/l of radon daughters were observed under conditions of inversion[37], and in such a case a field measurement here would overestimate the concentration of ^{226}Ra in the soil by approximately 20%. In cases of normal atmospheric turbulence, however, the overestimates are negligible.

6.4.5. Discussion of Exposure Rate Estimates

The validity of the exposure rate estimates from the spectroscopic measurements in the field is tested by comparing the terrestrial exposure rates to the total exposure rates and observing the difference between the two. Under the assumption that the estimated exposure rates adequately describe the true ones, this difference must be interpreted as the exposure rate in air from the cosmic radiation at sea level, because the altitude above sea level at each of the sites was less than 100 m.

As seen from table 6.4.1.3, a remarkable consistency characterizes the difference between the two exposure rates for the sites, especially considering the large variations in the total exposure rate estimates. This indicates that the exposure rate

from terrestrial sources is adequately accounted for by the estimates of exposure rate from the individual natural sources, and it thus supports the results of the field measurements.

The mean value of 4.18 ± 0.04 μR/h for the difference is in agreement with the 95% confidence interval of the zero intercept (3.83-4.27 μR/h) from the calibration of the NaI(Tl) detector used as a total count scintillometer described in section 4.3. . It must also be noted that the value of the zero intercept of 4.05 μR/h represents a slight underestimation of the total exposure rate in air, without the presence of terrestrial sources, because of the small response of the NaI(Tl) detector to cosmic-ray secondaries[7], and because of the small contribution from the potassium in the detector assembly.

The exposure rate of 4.18 μR/h, however, is 16% higher than the value for the total cosmic-ray ionization in air at sea level adopted by UNSCEAR[38], but even the most recently reported ionization chamber measurements differ by 30-40%, and an average of eight reported values since 1960 is equivalent to 4.21 μR/h[39].

The assumption of the validity of the exposure rate estimates from the Ge(Li) spectrometer system is therefore accepted.

6.5. Performance of Equipment in the Field

The only major practical problem encountered concerns the operation of the Ge(Li) detector under varying weather conditions. The stability of the system is affected by temperature variations at the preamplifier, but when the preamplifier has adjusted to the outdoor temperature, no significant changes in the detector resolution are observed with counting times of up to 3 hours. In cases of high humidity in the air, however, the system becomes inoperable due to electrical noise, that originates from leakage currents between the electrical connections to the detector, which is supplied with a high voltage of 3.5 kV. The electrical noise effect was observed during measurements in foggy weather and during heavy rainfall. It is therefore planned to provide an airtight packing for the preamplifier and the connections to the cryostat.

7. SUMMARY AND CONCLUSIONS

A mobile spectrometer system for field measurements of environmental gamma radiation using Ge(Li) and NaI(Tl) detectors was described. The methods for the evaluation of the recorded gamma-ray spectra were outlined and the results of the calibrations presented.

A computer program for the analysis of the recorded Ge(Li) spectra was worked out and its performance evaluated by the analyses of test spectra provided by the International Atomic Energy Agency. In the case of single peaks, the results proved satisfactory, while for doublets the results deviated more from the true values than the calculated errors could account for. This is probably explained by the use of a simple Gaussian representation of the peaks. An investigation of this can be made by the incorporation of a more complex fitting function in the program.

The intended test of the results of the Ge(Li) measurements with the results of the NaI(Tl) measurements was not accomplished because of problems with the calibration of the NaI(Tl) detector.

A great number of soil samples from all over the country were investigated for the state of equilibrium in the ^{238}U series and an average ratio of 0.96 ± 0.11 between the amounts of ^{226}Ra and the amounts of ^{238}U was obtained.

The validity of the results from a series of repeated measurements with the Ge(Li) spectrometer system at a single locality was confirmed by the comparison to laboratory measurements of collected soil samples. The results of the field measurements were also compared with the results of laboratory measurements of soil samples prepared for the determination of accumulated fallout. This revealed significant differences for the naturally occurring radionuclides, while for ^{137}Cs the results were in reasonable agreement. The observed disagreements are probably explained by the removal of moisture and stones from the collected soil samples.

A series of country-wide field measurements made in June 1977 yielded average ^{95}Zr and ^{95}Nb concentrations of 2.1 and 3.4 mCi/km^2, respectively, resulting from the atmospheric nuclear

weapons test performed on 17 November 1976 by the People's Republic of China. The results for the naturally occurring radionuclides from the field measurements were compared with those from laboratory measurements of collected soil samples prepared for detection of fallout. The differences were highly significant. Also in this case the explanation was believed to lie in the removal of considerable portions of the collected soil samples. Measurements were made at each site of the total exposure rate, which was compared to the exposure rate from terrestrial sources as estimated from the spectroscopic measurements. The validity of these estimates was strongly supported because the difference, caused mainly by the cosmic ray contribution, between the two exposure rates proved practically invariant (4.2 μR/h) for all the sites.

ACKNOWLEDGEMENTS

The author wishes to thank H. Mundt for help in practical matters, Jytte L. Clausen for performing the analyses of the soil samples and Karen W. Nielsen for assistance with calibration of the Ge(Li) detector.

He is greatly indebted to A. Aarkrog for many fruitful discussions, and especially to J. Lippert who as the author's tutor gave valuable support throughout this work.

REFERENCES

1) L.R. Solon et al., Investigations of Natural Environmental Radiation. Science 131 (1960) 903-906.

2) A. Shambon, W.M. Lowder, and W.J. Condon, Ionization Chambers for Environmental Radiation Measurements. HASL-108 (1963) 39 pp.

3) H.L. Beck, W.J. Condon, and W.M. Lowder, Spectrometric Techniques for Measuring Environmental Gamma Radiation. HASL-150 (1964) 71 pp.

4) R.A. Keil and T. Franke, Calculation of the Radiation Dose Resulting from Natural and Artificial Radioisotopes in the Ground by Gamma-Ray Spectrometry. Paper presented at the Fourth Symposium on Radioactivity in Scandinavia, Risø, Denmark, 5-6 October 1964. 12 pp.

5) S. Moriuchi and I. Miyanaga, A Spectrometric Method for Measurement of Low-Level Gamma Exposure Dose. Health Phys. 12 (1966) 541-551.

6) J. Pensko, Dosimetry of Environmental Gamma-Radiation in Poland by Means of Gamma-Ray Spectra in the Field. CLOR-48/D (1966) 27 pp.

7) H.L. Beck, J. DeCampo and C. Gogolak, In Situ Ge(Li) and NaI(Tl) Gamma-Ray Spectrometry. HASL-258 (1972) 75 pp.

8) L.R. Anspaugh et al., The In-Situ Measurement of Radionuclides in the Environment with a Ge(Li) Spectrometer. In: Proceedings of the Second International Symposium on the Natural Radiation Environment, Houston, Texas, 7-11 August 1972. Edited by J.A.S. Adams, W.M. Lowder, and T.F. Gesell (ERDA, Washington, 1972) (CONF-720805-P1) 279-303.

9) H.W. Dickson et al., Environmental Gamma-Ray Measurements using In Situ and Core Sampling Techniques. Health Phys. 30 (1976) 221-227.

10) E. Sakai, H. Terada, and M. Katagiri, In Situ Gamma-Ray Measurements using Ge(Li) Detectors. IEEE Trans. Nucl. Sci. NS-23 (1976) 726-733.

11) R.R. Finck, K. Lidén, and R.B.R. Persson, In Situ Measurements of Environmental Gamma Radiation by the use of a Ge(Li)-Spectrometer. Nucl. Instrum. Methods 135 (1976) 559-567.

12) J.A. DeCampo, H.L. Beck, and P.D. Raft, High Pressure Argon Ionization Chamber Systems for the Measurement of Environmental Exposure Rates. HASL-260 (1972) 73 pp.

13) H.L. Beck, Environmental Gamma Radiation from Deposited Fission Products, 1960-1964. Health Phys. 12 (1966) 313-322.

14) H.L. Beck, The Absolute Intensities of Gamma-Rays from the Decay of ^{238}U and ^{232}Th. HASL-262 (1972) 14 pp.

15) L. Løvborg and P. Kirkegaard, Response of 3" x 3" NaI(Tl) Detectors to Terrestrial Gamma Radiation. Nucl. Instrum. Methods 121 (1974) 239-251.

16) Z.G. Burson and A.E. Profio, Structure Shielding from Cloud and Fallout Gamma-Ray Sources for Assessing the Consequences of Reactor Accidents. EGG-1183-1670 (1975) 38 pp.

17) H.L. Beck and G. de Planque, The Radiation Field in Air due to Distributed Gamma-Ray Sources in the Ground. HASL-195 (1968) 53 pp.

18) H.L. Beck, Gamma Radiation from Radon Daughters in the Atmosphere. J. Geophys. Res. 79 (1974) 2215-2221.

19) L. Løvborg, P. Kirkegaard, and I. Rose-Hansen, Quantitative Interpretation of the Gamma-Ray Spectra from Geologic Formations. In: Proceedings of the Second International Symposium on the Natural Radiation Environment, Houston, Texas, 7-11 August 1972. Edited by J.A.S. Adams, W.M. Lowder, and T.F. Gesell (ERDA, Washington, 1972) (CONF-720805-P1) 155-180.

20) A.R. Smith and H.A. Wollenberg, High-Resolution Gamma-Ray Spectrometry for Laboratory Analysis of the Uranium and Thorium Decay Series. In: Proceedings of the Second International Symposium on the Natural Radiation Environment, Houston, Texas, 7-11 August 1972. Edited by J.A.S. Adams, W.M. Lowder, and T.F. Gesell (ERDA, Washington, 1972) (CONF-720805-P1) 181-231.

21) L. Løvborg, L. Bøtter-Jensen, and P. Kirkegaard, Experiences with Concrete Calibration Sources for Radiometric Field Instruments, to be published in Geophysics, April 1978.

22) J. Lippert, A B6700 Program for Handling and Statistical Treatment of Measurement Results. Risø-M-1780 (1975) 67 pp.

23) P.A. Baedecker, Digital Methods of Photopeak Integration in Activation Analysis. Anal. Chem. 43 (1971) 405-410.

24) A. Savitzky and M.J.E. Golay, Smoothing and Differentiation of Data by Simplified Least Squares Procedures. Anal. Chem. 36 (1964) 1627-1639.

25) H.P. Yule, Data Convolution and Peak Location, Peak Area, and Peak Energy Measurements in Scintillation Spectrometry. Anal. Chem. 38 (1966) 103-105.

26) H.P. Yule, Mathematical Smoothing of Gamma-Ray Spectra. Nucl. Instrum. Methods 54 (1967) 61-65.

27) V. Barnes, GASPAN - An Advanced Computer Code for the Analysis of High Resolution Gamma-Ray Spectra. IEEE Trans. Nucl. Sci. NS-15 No. 3 (1968) 437-454.

28) M.L. Verheijke, A Computer Program in Algol-60 for the Location and Evaluation of Peaks in Ge(Li) Gamma-Ray Spectra. J. Radioanal. Chem. 10 (1972) 299-314.

29) K. Madsen, Optimering. 2. udgave. Danmarks Tekniske Højskole, Numerisk Institut, hæfte 38 (1976) 28 pp.

30) P.R. Bevington, Data Reduction and Error Analysis for the Physical Sciences. (McGraw-Hill, New York, 1969) 334 pp.

31) J.E. Cline, H.M. Putnam, and R.G. Helmer, Gauss IV - A Computer Program for the Automatic Batch Analysis of Gamma-Ray Spectra from Ge(Li) Spectrometers. ANCR-1113 (1973) 76 pp.

32) L.T. Felawka et al., GAMAN - A Computer Program for the Qualitative and Quantitative Evaluation of Ge(Li) Gamma-Ray Spectra. [illegible]L-4217 (1973) 88 pp.

33) J.I. Routti and S.G. Prussin, Photopeak Method for the Computer Analysis of Gamma-Ray Spectra from Semiconductor Detectors. Nucl. Instrum. Methods 72 (1969) 125-142.

34) R.G. Helmer et al., Photopeak Analysis Program for Photon Energy and Intensity Determinations. Nucl. Instrum. Methods 57 (1967) 46-57.

35) L. Løvborg, Risø, Denmark, Personal communication, 1977.

36) L. Løvborg, H. Kunzendorf, and E. Mose Christiansen, Practical Experiences of Various Nuclear Techniques Supporting Mineral Prospecting in Greenland. In: Nuclear Techniques in Geochemistry and Geophysics. Proceedings of a Panel on Nuclear Techniques in Geochemistry and Geophysics held by the International Atomic Energy Agency in Vienna, 25-29 November 1974 (IAEA, Vienna, 1976) 139-152.

37) S.P. Nielsen, Risø, Denmark, unpublished work, 1974.

38) Ionizing Radiation: Levels and Effects. A report of the United Nations Scientific Committee on the Effects of Atomic Radiation. Vol. 1 (United Nations, New York, 1972) 197 pp.

39) D.T. Oakly and A.S. Goldin, Cosmic Ray Population Exposure. In: Proceedings of the Second International Symposium on the Natural Radiation Environment, Houston, Texas, 7-11 August 1972. Edited by J.A.S. Adams, W.M. Lowder, and T.F. Gesell (ERDA, Washington, 1972) (CONF-720805-P1) 91-99.

APPENDIX

DERIVATIONS OF THE UNCOLLIDED GAMMA FLUX ABOVE GROUND PER UNIT CONCENTRATION OF SOURCE FOR VARIOUS DISTRIBUTIONS

1. Exponentially Distributed Source

The flux is given by the expression

$$\phi = \int_0^{\pi/2} \int_{\frac{h}{\cos\theta}}^{\infty} \frac{S_o \exp[-\alpha(R\cos\theta - h)]}{4\pi R^2} \exp[-\mu_a h/\cos\theta - \mu_s(R - h/\cos\theta)] \cdot 2\pi R^2 \sin\theta \, dR \, d\theta. \quad (1)$$

By rearranging we obtain

$$\phi = S_o/2 \int_0^{\pi/2} \exp(-\mu_a h/\cos\theta) \sin\theta \int_{\frac{h}{\cos\theta}}^{\infty} \exp[-\alpha(R\cos\theta - h) - \mu_s(R - h/\cos\theta)] \, dR \, d\theta \quad (2)$$

$$= S_o/2 \int_0^{\pi/2} \exp(-\mu_a h/\cos\theta) \sin\theta \int_{\frac{h}{\cos\theta}}^{\infty} \exp[-(\alpha\cos\theta + \mu_s)R + (\alpha + \mu_s/\cos\theta)h] \, dR \, d\theta. \quad (3)$$

The R-integration is of the form

$$\int \exp(ax + b) \, dx = a^{-1} \exp(ax + b) ,$$

and we therefore obtain for the last integral in equation (3):

$$\left[\frac{\exp[-(\alpha\cos\theta + \mu_s)R + (\alpha + \mu_s/\cos\theta)h]}{-(\alpha\cos\theta + \mu_s)} \right]_{\frac{h}{\cos\theta}}^{\infty}$$

$$= \frac{\exp[-(\alpha\cos\theta + \mu_s)\, h/\cos\theta + (\alpha + \mu_s/\cos\theta)h]}{\alpha\cos\theta + \mu_s}$$

$$= \frac{1}{\alpha\cos\theta + \mu_s} .$$

Inserting this in equation (3) yields

$$\phi = \int_0^{\pi/2} \frac{d\phi}{d\theta}\, d\theta ,$$

where

$$\frac{d\phi}{d\theta} = \frac{S_o \sin\theta \exp(-\mu_a h/\cos\theta)}{2(\alpha\cos\theta + \mu_s)} . \qquad (4)$$

By substituting $u = \cos\theta$, $du = -\sin\theta\, d\theta$ we have

$$\phi = \frac{S_o}{2} \int_0^1 \frac{\exp(-\mu_a h/u)}{\alpha u + \mu_s} du. \qquad (5)$$

The variable is further substituted by $v = \mu_a h/u$, $dv = -\mu_a h/u^2\, du$, which yields for equation (5):

$$\phi = \frac{S_o}{2} \mu_a h \int_{\mu_a h}^{\infty} \frac{\exp(-v)}{(\alpha\mu_a h/v + \mu_s)v^2} dv \qquad (6)$$

$$= \frac{S_o}{2} \mu_a h \int_{\mu_a h}^{\infty} \exp(-v)\left[\frac{1}{\alpha\mu_a h v} - \frac{1}{\alpha\mu_a h(\alpha h\mu_a/\mu_s + v)}\right] dv \qquad (7)$$

$$= \frac{S_o}{2\alpha} \int_{\mu_a h}^{\infty} \frac{\exp(-v)}{v} dv - \frac{S_o}{2\alpha} \int_{\mu_a h}^{\infty} \frac{\exp(-v)}{v + \alpha h\mu_a/\mu_s} dv. \qquad (8)$$

Substituting $x = v + \alpha h\mu_a/\mu_s$, $dx = dv$ for the last integral yields

$$\phi = \frac{S_o}{2\alpha} \int_{\mu_a h}^{\infty} \frac{\exp(-v)}{v} dv - \frac{S_o}{2\alpha} \exp(\alpha h \frac{\mu_a}{\mu_s}) \int_{\mu_a h + \alpha h \mu_a/\mu_s}^{\infty} \frac{\exp(-x)}{x} dx. \quad (9)$$

By introducing the exponential integral of n'th order defined by

$$E_n(t) = t^{n-1} \int_t^{\infty} \frac{\exp(-y)}{y^n} dy , \quad (10)$$

we obtain for equation (9):

$$\phi = \frac{S_o}{2\alpha} [E_1(\mu_a h) - \exp(\alpha h \mu_a/\mu_s) E_1(\mu_a h + \alpha h \mu_a/\mu_s)] . \quad (11)$$

2. Surface Deposited Source

The surface distribution is derived from the exponential distribution by letting $\alpha \to \infty$. This yields for the differential angular flux from equation (4):

$$\frac{d\phi}{d\theta} = \frac{S_o}{2\alpha} \tan\theta \exp(-\mu_a h/\cos\theta) , \quad (12)$$

and the flux is obtained by integration

$$\phi = \frac{S_o}{2\alpha} \int_0^{\pi/2} \tan\theta \exp(-\mu_a h/\cos\theta) \, d\theta . \quad (13)$$

By substituting $u = \mu_a h/\cos\theta$, $du = \mu_a h \sin\theta/\cos^2\theta \, d\theta = u \tan\theta \, d\theta$ we have

$$\phi = \frac{S_o}{2\alpha} \int_{\mu_a h}^{\infty} \frac{\exp(-u)}{u} du = \frac{S_o}{2\alpha} E_1(\mu_a h) . \quad (14)$$

3. Homogeneously Distributed Source

The homogeneous distribution is obtained from the exponential distribution for the case of $\alpha = 0$, which yields for the differential angular flux:

$$\frac{d\phi}{d\theta} = \frac{S_o}{2\mu_s} \sin\theta \exp(-\mu_a h/\cos\theta) \ . \qquad (15)$$

The flux is obtained by integration:

$$\phi = \frac{S_o}{2\mu_s} \int_o^{\pi/2} \sin\theta \exp(-\mu_a h/\cos\theta) \, d\theta \ , \qquad (16)$$

and by substituting $u=\mu_a h/\cos\theta$, $du=\mu_a h\sin\theta/\cos^2\theta \ d\theta=u^2\sin\theta/(\mu_a h)d\theta$ we have:

$$\phi = \frac{S_o}{2\mu_s} \mu_a h \int_{\mu_a h}^{\infty} \frac{\exp(-u)}{u^2} du = \frac{S_o}{2\mu_s} E_2(\mu_a h) \ . \qquad (17)$$

ISBN 87-550-0501-2
ISSN 0418-6443